Design and experiment of furrow side pick-up soil blade for wheat strip-till planter using the discrete element method

Lei Liu,[1] Xianliang Wang,[1] Xiaokang Zhong,[1] Xiangcai Zhang,[1] Yuanle Geng,[1] Hua Zhou,[1] Tao Chen[2]

[1]College of Agricultural Engineering and Food Science, Shandong University of Technology, Zibo; [2]Shandong Shengli Steel Pipe Co., Ltd., Zibo, China

Abstract

The strip rotary tillage method effectively reduces the occurrence of straw clogging and creates a favorable seed bed environment. However, the mixture of crushed straw and soil in the seeding area results in inadequate seed-soil contact following compaction by the press wheels. A chisel-type opener furrow side pick-up blade was proposed to improve seed-soil contact by picking up wet soil from the furrow's side. The discrete element method was used to investigate the impact of earth blade surface parameters on soil dynamics. The key factors of the blade, including forward velocity, endpoint tangent angle, and angle of soil entry, were determined through theoretical analysis. Soil cover thickness and straw ratio in the seed furrow were evaluated using orthogonal rotation regression tests. The results show that the endpoint tangent angle and angle of soil entry have the greatest influence on soil cover thickness, while the angle of soil entry has the greatest influence on the straw ratio. The optimal values for the forward velocity, endpoint tangent angle, and angle of soil entry are 4.86 km/h, 107.17°, and 5.46°, respectively, resulting in a soil cover thickness of 40 mm and a straw ratio of 21.46%. Confirmatory soil bin tests showed similar results, with a soil cover thickness of 40.4 mm and a straw ratio of 18.03%. These results provide a viable solution for improving seed-soil contact after strip rotary tillage planter seeding.

Correspondence: Xianliang Wang, College of Agricultural Engineering and Food Science, Shandong University of Technology, Zibo 255000, China.
E-mail: wxl1990@sdut.edu.cn

Key words: discrete element simulation; experimental design; straw returning; strip rotary tillage.

Contributions: the authors contributed equally.

Conflict of interest: the authors declare no potential conflict of interest.

Funding: this work was supported financially by the National Natural Science Foundation of China (Grant No. 32101631).

Acknowledgments: we are grateful to the editor and anonymous reviewers for providing helpful suggestions to improve the quality of this paper.

Received: 21 July 2023.
Accepted: 10 September 2023.

Journal of Agricultural Engineering 2024; LV:1546
doi:10.4081/jae.2023.1546

Introduction

Conservation tillage technology is one of the main technologies promoted by the Ministry of Agriculture and Rural Development in China, which has the advantages of protecting the ecological environment, improving soil fertility, improving soil tillage structure, alleviating deep soil compaction, and promoting sustainable development of agricultural production (Aikins *et al*., 2020). The wheat strip rotary tillage is the main mode of conservation tillage under full straw mulching in the Huanghuaihai wheat-maize double cropping region, an important grain producing area in China (Chen *et al*., 2018), which can solve the clogging of implements caused by full straw mulching, and create a loose seedbed environment for wheat as well as improve the ground temperature. Due to the large amount of straw coverage on the ground, the seed bed contains much straw during wheat strip rotary tillage sowing, and the soil-straw complex has too many loose pores for the seeds to be in full contact with the soil (Gu *et al*., 2016), resulting in problems such as seed cracking and drying, poor seed suppression, reduced wheat germination and growth, and finally causes a reduction in yield. Therefore, reducing the amount of straw coverage in the seed furrow is a prerequisite for ensuring the quality of no-till seeding.

To reduce the amount of straw cover on the surface, scholars have carried out a lot of research from different perspectives, such as optimizing the cleaning of straw in seed beds with a strip rotary tillage tool, evenly spraying of straw, and the covering process. Zhao *et al.* (2020) designed a rotary cutter with only a side cutting edge and applied the rotary cutter to a strip-type rotary cutting back throw anti-blocking device, achieving stubble reduction and cleaning. Zhao *et al*. (2018b) experimentally compared flat C-shaped rotary tillage blades with conventional C-shaped rotary tillage blades. It was found that for shallow soils, the soil mixing index was significantly higher with flat C-blades than with conventional blades and that most of the mixed soil moved into the adjacent layers. The conventional C-blade throws 19.2% of soil particles and 64.8% of straw from the seedbed, while the flat C-blade throws 15.0% and 61.8%, and the flat C-blade has lower torque requirements and soil resistance for a cleaner seedbed. Zhang *et al.* (2017) designed an adjustable straw crushing and

Design and experiment of furrow side pick-up soil blade for wheat strip-till planter using the discrete element method

Lei Liu,[1] Xianliang Wang,[1] Xiaokang Zhong,[1] Xiangcai Zhang,[1] Yuanle Geng,[1] Hua Zhou,[1] Tao Chen[2]

[1]College of Agricultural Engineering and Food Science, Shandong University of Technology, Zibo; [2]Shandong Shengli Steel Pipe Co., Ltd., Zibo, China

Abstract

The strip rotary tillage method effectively reduces the occurrence of straw clogging and creates a favorable seed bed environment. However, the mixture of crushed straw and soil in the seeding area results in inadequate seed-soil contact following compaction by the press wheels. A chisel-type opener furrow side pick-up blade was proposed to improve seed-soil contact by picking up wet soil from the furrow's side. The discrete element method was used to investigate the impact of earth blade surface parameters on soil dynamics. The key factors of the blade, including forward velocity, endpoint tangent angle, and angle of soil entry, were determined through theoretical analysis. Soil cover thickness and straw ratio in the seed furrow were evaluated using orthogonal rotation regression tests. The results show that the endpoint tangent angle and angle of soil entry have the greatest influence on soil cover thickness, while the angle of soil entry has the greatest influence on the straw ratio. The optimal values for the forward velocity, endpoint tangent angle, and angle of soil entry are 4.86 km/h, 107.17°, and 5.46°, respectively, resulting in a soil cover thickness of 40 mm and a straw ratio of 21.46%. Confirmatory soil bin tests showed similar results, with a soil cover thickness of 40.4 mm and a straw ratio of 18.03%. These results provide a viable solution for improving seed-soil contact after strip rotary tillage planter seeding.

Correspondence: Xianliang Wang, College of Agricultural Engineering and Food Science, Shandong University of Technology, Zibo 255000, China.
E-mail: wxl1990@sdut.edu.cn

Key words: discrete element simulation; experimental design; straw returning; strip rotary tillage.

Contributions: the authors contributed equally.

Conflict of interest: the authors declare no potential conflict of interest.

Funding: this work was supported financially by the National Natural Science Foundation of China (Grant No. 32101631).

Acknowledgments: we are grateful to the editor and anonymous reviewers for providing helpful suggestions to improve the quality of this paper.

Received: 21 July 2023.
Accepted: 10 September 2023.

Journal of Agricultural Engineering 2024; LV:1546
doi:10.4081/jae.2023.1546

Introduction

Conservation tillage technology is one of the main technologies promoted by the Ministry of Agriculture and Rural Development in China, which has the advantages of protecting the ecological environment, improving soil fertility, improving soil tillage structure, alleviating deep soil compaction, and promoting sustainable development of agricultural production (Aikins *et al*., 2020). The wheat strip rotary tillage is the main mode of conservation tillage under full straw mulching in the Huanghuaihai wheat-maize double cropping region, an important grain producing area in China (Chen *et al*., 2018), which can solve the clogging of implements caused by full straw mulching, and create a loose seedbed environment for wheat as well as improve the ground temperature. Due to the large amount of straw coverage on the ground, the seed bed contains much straw during wheat strip rotary tillage sowing, and the soil-straw complex has too many loose pores for the seeds to be in full contact with the soil (Gu *et al*., 2016), resulting in problems such as seed cracking and drying, poor seed suppression, reduced wheat germination and growth, and finally causes a reduction in yield. Therefore, reducing the amount of straw coverage in the seed furrow is a prerequisite for ensuring the quality of no-till seeding.

To reduce the amount of straw cover on the surface, scholars have carried out a lot of research from different perspectives, such as optimizing the cleaning of straw in seed beds with a strip rotary tillage tool, evenly spraying of straw, and the covering process. Zhao *et al.* (2020) designed a rotary cutter with only a side cutting edge and applied the rotary cutter to a strip-type rotary cutting back throw anti-blocking device, achieving stubble reduction and cleaning. Zhao *et al*. (2018b) experimentally compared flat C-shaped rotary tillage blades with conventional C-shaped rotary tillage blades. It was found that for shallow soils, the soil mixing index was significantly higher with flat C-blades than with conventional blades and that most of the mixed soil moved into the adjacent layers. The conventional C-blade throws 19.2% of soil particles and 64.8% of straw from the seedbed, while the flat C-blade throws 15.0% and 61.8%, and the flat C-blade has lower torque requirements and soil resistance for a cleaner seedbed. Zhang *et al.* (2017) designed an adjustable straw crushing and

spreading machine to return the straw to the field. During the operation process, the straw is finely crushed, and the information parameters such as the position, width, uniformity, and distance of the thrown straw are controlled and adjusted to regulate the straw cover state. Realize to clean the straw on the ground before planting to reduce the impact of the straw cover on planting. Liu *et al*. (2018b) designed a stubble cleaning device with a seed belt cleaning curved knife as the main working part to solve the problems of serious mixing of soil and straw, high seed drying rate, and poor sowing quality when sowing corn by strip rotary tillage. The field test verified that the machine passed well, the soil disturbance was low, and the cleanliness of the seed belt could reach more than 80%. Zhao *et al*. (2018a) developed a strip-type tillage and back-throwing anti-blocking device, which throws the straw between the seed rows during the crushing process, reducing the accumulation of straw in the seed bed area. Niu *et al*. (2017) designed a post-straw mulching wheat planter for sowing wheat on corn straw mulched land prone to clogging and seed drying, which can complete rotary tillage, seeding, soil covering, straw covering, suppression, and other processes once in the field. Based on the analysis of rototiller throwing and straw throwing movement, the structure and position parameters of the soil guide were determined, and the straw-soil sequential mulching was realized.

The aim of this study is to improve seed-soil contact and develop a furrow side pickup blade based on a chisel-type furrow opener for strip-tillage of wheat in the double-cropping area of wheat and corn in Huanghuaihai. By using the Discrete Element Method (DEM), we established a model for the interaction between soil, straw, and a furrow side pickup blade. This model allowed us to determine the optimal working parameters for the furrow side pickup blade. It provides a feasible technical solution for addressing the issue of seed-soil contact under straw cover.

Materials and Methods

Overall structure and working principle

The overall structure of the chisel opener furrow side pick-up blade is shown schematically in Figure 1. The main components of the system include the opener blade tip, the opener handles, and the curved surface of the furrow side pick-up blade. The latter is securely welded to both sides of the opener, ensuring the structural integrity and stability of the system.

During the tilling operation, the front end of the furrow side pick-up blade engages the soil level at a specific angle of soil entry. As the opener progresses, the soil located on both sides of the seed furrow is lifted along the curved surface of the furrow side pick-up blade, with the latter gradually inwardly curving front to back. The soil, after being turned over, rises to a certain height, at which point the curved surface exerts an inward extrusion effect upon the soil, resulting in a continuous turnover of the soil in contact with and adjacent to it. This culminates in the process of collecting and covering the wet soil from the side of the furrow.

The furrow side pick-up blade surface design

In this study, the horizontal element straight-line method was employed, which conceptualizes the surface of the plow body as a continuous surface constituted by horizontal element straight lines moving upward along a guide curve from the bottom surface. The length of this horizontal element straight line and the angle θ between them and the x-axis vary as the guide curve ascends (Lu *et al.*, 2020; Wei *et al.*, 2020). The surface of the plow body was constructed by the movement of the horizontal element straight lines along a horizontal trace, as illustrated in Figure 2a.

A Guide Curve Model was established, as depicted in Figure 2b. The determination of its shape is a crucial aspect of the design of the furrow side pick-up blade surface and is influenced by various factors, including the height of the curve (h), the opening (L), the starting angle (ε), the endpoint tangent angle (ω), and the length of the starting straight-line segment (s).

The determination of the height of the guide curve (h), representing the depth of cultivation, is a crucial aspect of the design of the furrow side pick-up blade surface. In this study, the height of the highest point of the surface was set to 50mm. The ploughing width (L), which represents the opening of the blade, was determined to be 90mm based on practical experience. The soil draft angle (ε) plays a critical role in the design of the furrow side pick-up blade surface. A larger soil draft angle leads to a shorter soil extraction blade and greater tillage resistance. Based on empirical evidence, the soil draft angle was set to 25°, with a range of 20-30°. Furthermore, the endpoint tangent angle (ω) also influences the performance of the furrow side pick-up blade. A larger endpoint tangent angle results in greater wing twists and improved soil-turning effects. The endpoint tangent angle is determined by the inclination angle (Δε) at the end of the guide curve and the starting angle (ε), as described by the following formula:

$$\omega = \frac{\pi}{2} + \varepsilon - \Delta\varepsilon \quad (1)$$

According to the design specifications outlined in the "Agricultural Machinery Design Manual" the range of the derivative curve, Δε, is typically between 0° and 10°. As such, the angular velocity, ω, which serves as a key experimental variable, is set to values ranging from 106° to 110°.

The variation of the element line angle, θ, is illustrated in Figure 2c. The variation law of θ displays two distinctive segments, exhibiting a trend of first decreasing and then increasing. The initial segment is linear, with its starting point represented by θ_0, which generally falls within the range of 35° to 40°. The minimum value of the element line angle, θ_{min}, can be calculated as θ_0-(2° to 4°), with a sample value of 38°. The second segment is curved, for which a parabolic function has been chosen to model the soil turning surface. The curve function is expressed as $\theta_{max}=\theta_0+(7°$ to $15°)$, with a sample value of 50°.

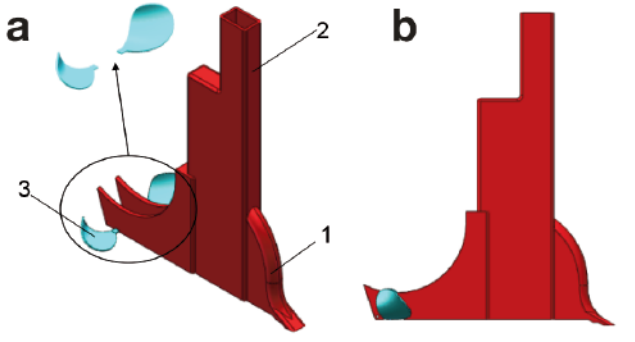

Figure 1. Schematic diagram of the overall structure: **a**) the overall structure; **b**) side view; 1) opener blade tip; 2) opener handle; 3) the furrow side pick-up blade curved surface.

Force analysis of the angle of soil entry

The soil extraction section of the soil covering operation requires precise guidance at the outset to ensure that the cut soil can effectively leap up and lift the moist soil from the furrow bottom to the surface, while simultaneously facilitating the accumulation of a substantial amount of soil. The front end of the furrow side pick-up blade undergoes a force analysis, as depicted in Figure 2d.

In Figure 2d, N_0 represents the positive pressure reaction force exerted on the front section of the furrow side pick-up blade, T_0 denotes the friction force acting on the working surface, R_0 represents the resultant force generated by the combination of N_0 and T_0, φ represents the friction angle, F_0 represents the forward direction component force of N_0, ε_0 represents the angle of soil entry and the angle of soil entry clearance, and β represents the angle of soil clearance. When the opener moves at a constant velocity, the forward direction component force F_0 of the soil access portion's positive pressure N_0 remains constant and is equal to the soil resistance of the furrow side pick-up blade at a specific depth. As a result, the working surface's force R_0 can be indirectly estimated through the combined force of surface positive pressure N_0 and frictional force T_0 (Lv *et al.*, 2021).

The vertical component R_{0Z} of the soil reaction force in the front section of the furrow side pick-up blade is:

$$R_{0z} = F_0 \sin\varepsilon_0 \cos\varepsilon_0 - F_0 \sin\varepsilon_0 \tan\varphi \sin\varepsilon_0 = F_0\left[\frac{\sin(2\varepsilon_0)}{2} - \sin^2(\varepsilon_0)\tan\varphi\right] \quad (2)$$

The component R_{0X} of the soil reaction force in the front section of the furrow side pick-up blade in the horizontal direction is:

$$R_{0X} = F_0 \sin\varepsilon_0 \sin\varepsilon_0 + F_0 \sin\varepsilon_0 \tan\varphi \cos\varepsilon_0 = F_0\left[\sin^2(\varepsilon_0) + \frac{\sin(2\varepsilon_0)}{2}\tan\varphi\right] \quad (3)$$

In the formula ε_0, the angle of soil entry and the angle of soil entry clearance (°).

For the furrow side pick-up blade, reducing the horizontal component of the soil reaction force on its front section can effectively improve the soil entry performance of the tool, so the above formula is derived:

$$R'_{0X} = \sin(2\varepsilon_0) + \cos(2\varepsilon_0)\tan\varphi \quad (4)$$

Since φ is the friction angle, that is, tan φ is a fixed value, the smaller the value of ε_0, the better. Therefore, the angle of soil entry clearance β is selected as one of the test factors, and its value ranges from 0° to 10°.

Surface force analysis

In the soil extraction process, the turning of soil is the main operation, and based on this effect, the stress situation of the soil during the turning process is analyzed utilizing the three-sided wedge simplification principle as depicted in Figure 2e1. The assumption is made that the three-sided wedge moves at a constant velocity in the positive direction of the x-axis. In Figure 2e1, α represents the soil starting angle, β represents the soil turning angle, γ represents the bulldozing angle, and point m is taken on the surface. The primary forces at point m include the soil pressure N and the total friction force T between the soil and the wedge surface, and R is the resultant of N and T. When the wedge surface moves

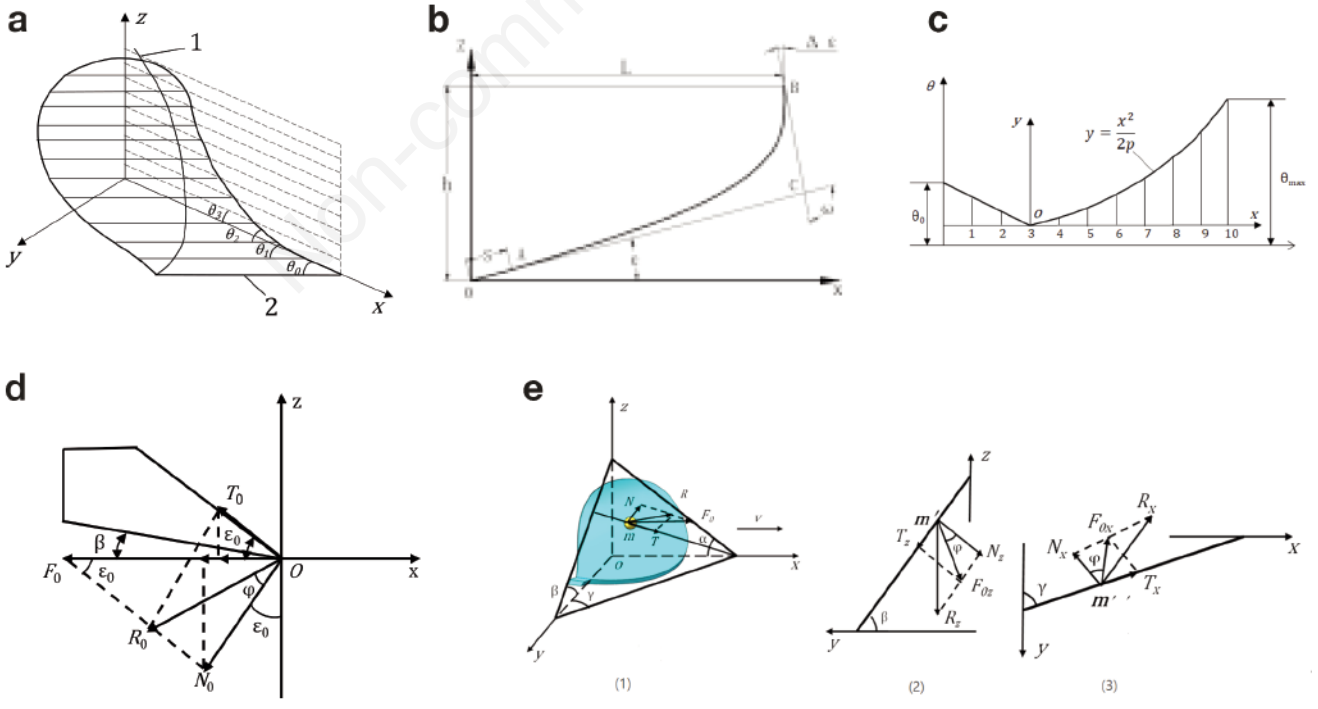

Figure 2. Theoretical analysis: **a**) the furrow side pick-up blade; 1) the guide curve; 2) the horizontal element straight line; **b**) model of guide curve of the furrow side pick-up blade surface; **c**) variation curve of line angle of the furrow side pick-up blade surface element; **d**) force analysis of the front end of the furrow side pick-up blade; **e**) force analysis on the surface of the furrow side pick-up blade.

at a constant velocity, the soil resistance in the horizontal direction on the wedge surface is equivalent to the forward component force F_0 of the positive pressure. Utilizing the analysis principle of the soil entry angle, the soil resistance F_0 can be employed to symbolize the force on the wedge surface (Zhai, 2011).

In Figure 2e2, the projection of the force at point m onto the yoz plane results in the force at point m' in the vertical section. The force at point m' can be represented by the following equation:

$$\begin{cases} N_z = R_z cos\beta = F_0(\frac{sin(2\alpha)}{2} - sin^2\alpha tan\varphi)cos\beta \\ T_z = R_z cos\beta tan\varphi = F_0(\frac{sin(2\alpha)}{2} - sin^2\alpha tan\varphi)cos\beta tan\varphi \end{cases} \quad (5)$$

In the formula: β is yoz face wedge angle, that is, turning the soil angle, (°); N_Z is yoz dihedral wedge pressure, (N); T_Z is yoz dihedral wedge friction, (N).

Projecting the above two-component force to the xoy plane, as shown in Figure 2e3, the soil reaction force of m'' on the horizontal plane can be obtained as:

$$R_l = F_0(\frac{sin(2\alpha)}{2} - sin^2\alpha tan\varphi)(cos^2\gamma + \frac{sin\,(2\gamma)}{2} tan\varphi) \quad (6)$$

In the formula γ is xoy face wedge angle, that is, the bulldozer angle, (°)

Simulation test

Soil model calibration

Fu (2008) and Sun (2009) found in their research that the smaller the particle radius, the smaller the error of the simulation experiment and physical experiment, but the calculation time will be doubled. The larger the particle radius, the faster the stress propagation between particles. After comprehensive consideration, soil particles with a particle radius of 5mm were selected with reference to Shi *et al.* (2017) on the premise of ensuring accuracy. The parameters of the soil particle model were mainly obtained with reference to the literature of the same soil type (Ding *et al.*, 2017; Wang *et al.*, 2017; Xiong *et al.*, 2018; Zhang *et al.*, 2009; Zhao *et al.*, 2019). The choice of contacting model has a great impact on the accuracy of soil discrete element simulation results. Wu *et al.* (2017) have proved that the Hertz-Mindlin with Johnson-Kendall-Roberts contact model is better than the traditional Hertz contact model. The model comprehensively considers the elastic deformation of soil particles and adds the influence of the cohesive force of the interaction between particles based on Hertz's theory. The value of the main parameter in the model, surface energy, is related to the amount of bond strength, which in turn determines the degree of soil fragmentation of the opener during tillage. In this paper, a soil accumulation angle test was adopted to verify the parameters under the condition of 15.8% soil moisture content. The simulation parameters of the model are shown in Table 1.

The soil accumulation angle test is composed of funnel, bracket, and receiving plate. The bottom of the funnel is 300mm away from the receiving plate. During the test, the lower end of the funnel is close to a thin plate, and the soil samples to be tested are evenly distributed into the funnel, followed by rapid withdrawal of the thin plate. The soil naturally falls from the funnel to the receiving plate under the action of gravity, and when the soil accumulation shape is stable, the digital display angle ruler is used to measure the soil accumulation angle from three directions. The above test is repeated five times, and the arithmetic average of the accumulated angle five times is taken as the final test result, the size of which is 38.5°, as shown in Figure 3a. The funnel model of actual size was established and imported into EDEM (Altair Engineering, Troy, MI, USA). The receiving plate was placed at the bottom of the funnel, and the relative position between the two was adjusted to be consistent with the real situation. Waiting for the particles to move in the catch plate until all the particles are relatively stable and form a stable pile of particles for post-processing, the measurement result is 38.8°, as shown in Figure 3b.

Modelling the straw structure

In the construction of the discrete element model for straw, multiple spherical surfaces of varying sizes and positions are established to form a strip model that closely resembles corn straw. This is achieved through stacking the spherical surfaces, with a 50% overlap between adjacent spheres serving as a compromise between surface resolution and computational efficiency. Referring to the method of selecting straw models in Itasca (2005), Chandio (2013), and Barker and Plouffe (2017), the furrow side pick-up blade designed in this paper pushes rather than cuts the straw, so the straw is also established as rigid. In this study, 20 corn stalks were randomly selected from the field of measurement and calculation. The discrete element model was constructed with 9 particles with a radius of 8mm and a length of 48 mm per stalk, and a total of 1843 corn stalks were randomly distributed in the topsoil layer. The Hertz-Mindlin (no slip) contact model was used to model the mechanical relationship between straw particles, based on the properties of crushed corn stalks returned to the field (Zhong *et al.* 2023). The parameters for the straw were obtained from relevant references (Zhao *et al.*, 2021; Zhang *et al.*, 2018; Yu *et al.*, 2018) and are shown in Table 2. The straw particle model is shown in Figure 3c.

Table 1. Soil particle parameters.

Parameter	Value
Soil solids density of particles ρ/(kg·m^{-3})	1680
Soil particle bonding radius r/mm	5.67
Soil shear modulus G/MPa	1
Poisson's ratio: soil ν	0.3
Coefficient of restitution soil-soil e	0.56
Coefficient of static friction soil-soil μ_s	0.79
Coefficient of rolling friction soil-soil μ_r	0.22
Soil JKR surface energy/(J·m^{-2})	8.06

JKR; Johnson-Kendall-Roberts contact model.

Table 2. Parameters of straw particles.

Parameter	Value
Straw solids density of particles ρ/(kg·m^{-3})	241
Poisson's ratio: straw ν	0.4
Straw shear modulus G/MPa	1
Coefficient of restitution straw-soil e	0.6
Coefficient of static friction straw-soil μ_s	0.537
Coefficient of rolling friction straw-soil μ_r	0.16
Coefficient of restitution straw-straw e	0.485
Coefficient of static friction straw-straw μ_s	0.213
Coefficient of rolling friction straw-straw μ_r	0.098

Modelling the wheat grain structure

In this study, the wheat grain model was established using Jimai 22. 100 full, undamaged, and pest-free wheat grains were randomly selected, and their triaxial diameter was measured using a vernier caliper, with the average value taken as the representative size (Liu *et al.*, 2016). The average geometric size of the wheat grains was found to be 5.1 mm in length, 2.8 mm in width, and 3.8mm in height. Since the surface of the wheat grains was smooth and fluid, it was assumed to be a uniform linear elastic material with homogeneous properties. The multi-sphere method was adopted to construct a double ellipsoid model of the wheat grain, as it was found to describe the actual wheat grains more accurately, based on the research of Sun *et al*. (2022) and Zhang *et al*. (2010). The wheat grain was simplified into 5 ball-bonded combined grains, piled up by 5 grains with different radii, with a total length of 5mm, as shown in Figure 3d-e. As the wheat grains are approximately ellipsoidal and exhibit no adhesion force on their surface, the Hertz-Mindlin (no-slip) non-slip contact model was selected as the material movement contact model. Other parameters of the grains were obtained by referencing relevant literature (Zhao *et al.*, 2018c; Liu *et al.*, 2018a), as shown in Table 3.

Discrete element modeling

In the simulation experiment, a virtual test soil bin was established with dimensions of 2000 mm in length, 1000 mm in width, and 200mm in depth. The choice of a 2000 mm length for the soil bin serves to stabilize the movement of the opener and provide sufficient data collection length. The 1000 mm width accommodates sufficient lateral particle movement to prevent excessive particles from flowing back into the seed furrow. The 200 mm depth allows for a tillage depth of 50mm with an adequate margin below to simulate actual soil conditions. To ensure the validity of the simulation, soil particles in the tillage layer and straws were generated randomly. During the simulation, a grain factory for wheat grains was established at the rear end of the opener and generated a total of 300 wheat grains through the interaction of the opener movement and the grain factory (Bai *et al.*, 2020). For the simulation experiment, the forward speed of the opener was set to 5 km/h, the endpoint tangent angle was set to 108°, and the soil entry angle was set to 5°.

Table 3. Wheat grain parameters.

Parameter	Value
Grain solids density of particles ρ/(kg·m^{-3})	1373
Poisson's ratio: soil ν	0.42
Grain shear modulus G/MPa	1.45
Coefficient of restitution grain-soil e	0.05
Coefficient of static friction grain-soil μ_s	1.25
Coefficient of rolling friction grain-soil μ_r	1.25
Coefficient of restitution grain-grain e	0.35
Coefficient of static friction grain-grain μ_s	0.3
Coefficient of rolling friction grain-grain μ_r	0.25
Coefficient of restitution grain-straw e	0.2
Coefficient of static friction grain-straw μ_s	0.8
Coefficient of rolling friction grain-straw μ_r	0.01
Coefficient of restitution grain-steel e	0.6
Coefficient of static friction grain-steel μ_s	0.5
Coefficient of rolling friction grain-steel μ_r	0.01

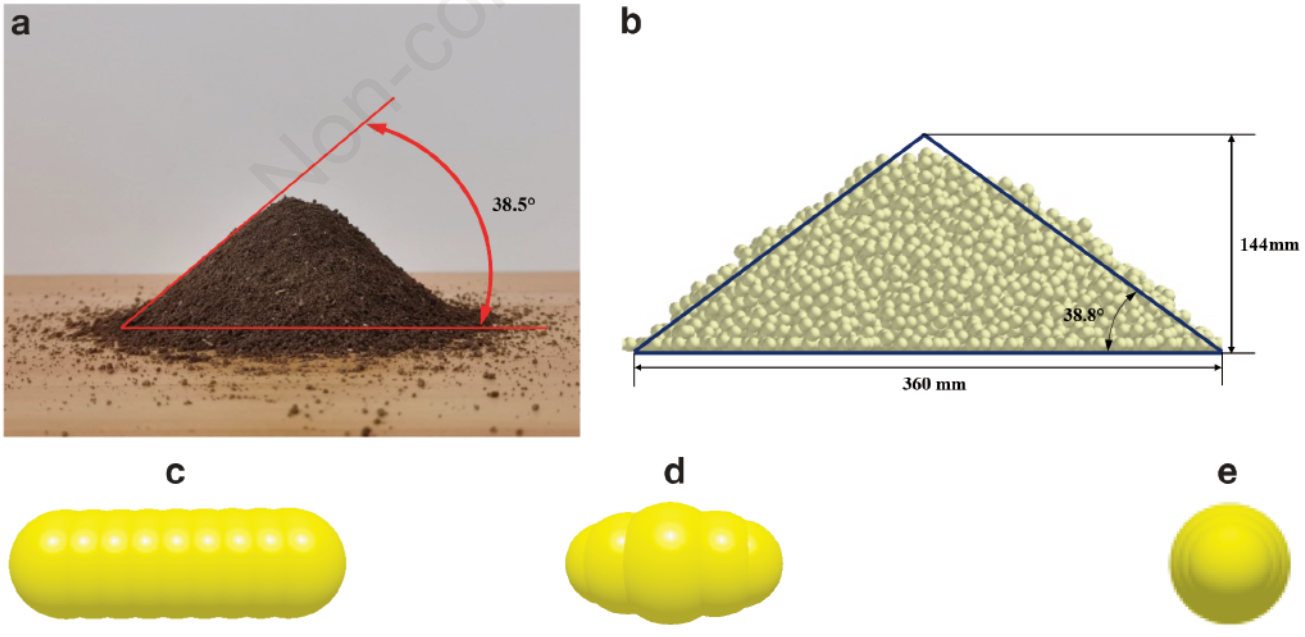

Figure 3. Calibration process. **a**) Soil accumulation angle actual; **b**) soil accumulation angle discrete element simulation; **c**) discrete element model of straw particles; **d**) wheat grain front view; **e**) side view.

Soil bin test

The experiment was conducted in the indoor soil bin of the Conservation Tillage Technology and Intelligent Equipment Innovation Laboratory at the Shandong University of Technology. The soil bin was 6 meters in length, 2 meters in width, and 0.7 meters in depth, and consisted of fluvo-aquic soil with an added appropriate amount of corn straw to simulate a straw-soil mixed environment. The soil moisture content was measured at 15.8% using the drying method, ensuring consistent test conditions throughout the plot.

Based on actual field environments, a two-layer soil model was established consisting of a bottom layer of pure soil particles with a depth of 150mm and a tillage layer mixed with soil and straw particles, having a depth of 50mm and a straw content of 30%. The depth of entry of the opener is 50 mm (Figure 4b). The operating conditions of the soil bin experiment were set to be the same as the simulation experiment, with the forward velocity of the opener being 5 km/h, the endpoint tangent angle being 108°, and the soil entry angle being 5°. The simulation results were compared with the actual data of the soil bin for the soil cover thickness and the straw ratio of the seed furrow.

The furrow side pick-up blade utilized in the experiment was fabricated using 3D printing technology and made of PLA material, with a manufacturing accuracy of 0.1mm. The remaining test equipment included a chisel opener, TYD-2 soil compaction meter, vernier caliper, tape measure, electronic scale, soil sampling ring knife, and drying oven.

Five locations were randomly selected observation areas in the operational travel stability zone of the test area (Figure 4c) and the soil height above the wheat seeds was measured using digital vernier calipers (resolution 0.02 mm) and the average value was obtained as the soil cover thickness. The results of the simulated test soil cover thickness were measured by measuring the height difference between the coordinates of wheat seeds and surface soil

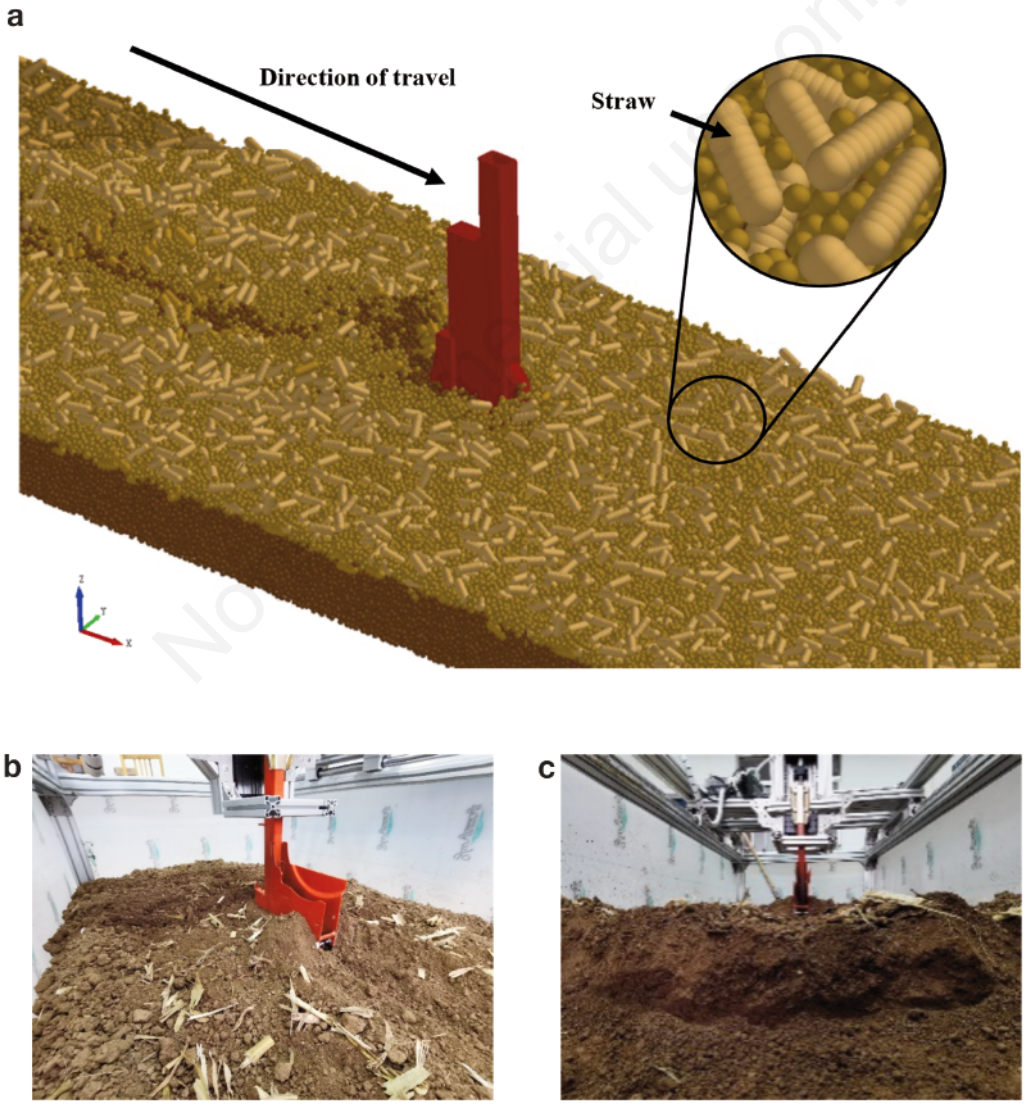

Figure 4. Experimentation. **a**) Axonometric view of opener through soil bin; **b**) test process; **c**) soil cover thickness measurement cross-section.

particles in the corresponding area selected by the EDEM post-processing module. The proportion of straw in the seed furrow, *i.e.*, the proportion of straw mass in the sampling area to all soil mass in the area, is the proportion of straw in the seed furrow, and the expression for the proportion of straw in the seed furrow is:

$$p = \frac{W_1}{W} \times 100\% \quad (7)$$

In the formula, ρ is the proportion of straw in the seed furrow, %

W_1 = Straw quality, g
W = the total mass of soil in the sampling area, g

After ditching in the test area, five sampling areas with the size of 300mm×200mm were randomly selected. The quality of soil and straw in the area was measured using a JA2003 electronic precision balance, and the five measurements were averaged. The straw mass and the total mass of the soil-straw complex in the selected area were derived from the EDEM post-processing module for calculation.

Experiment on optimal parameters of the furrow side pick-up blade

To further investigate the performance of the furrow side pick-up blade, the EDEM simulation model (Figure 4a) was used to determine the machine the forward velocity (v), the endpoint tangent angle (ω), and the soil entry angle (ε) as the test factors. The thickness of the covering soil and the ratio of straw in the seed furrow were used as evaluation indicators of the test. The optimal parameter combination for the furrow side pick-up blade was determined through a cross-rotation regression combination optimization test method. The codes for the test factors are presented in Table 4.

Results and Discussion

Model validation

DEM simulations were carried out using the software EDEM, 2020.0 (Academic Edition, Version: 6.0.0) working on a computer with AMD Ryzen 5 5600 G @ 3.90 GHz and 16.0 GB RAM.

The simulation results were compared with the results of the soil bin experiments. The average value of soil cover thickness predicted by the simulation experiment was 40.9 mm, and the average value of soil cover thickness measured by the soil bin test was 40.4 mm, with a single maximum error value of 2.26% (Figure 5a). The simulation test predicted a mean value of 17.69% of straw in the seed furrow, and the indoor soil bin test measured a mean value of 18.03% of straw in the seed furrow, with a single maximum error value of 2.86% (Figure 5b). The error of both results was within 5% and the trend was consistent, so it can be concluded that the model can better simulate the operation of the furrow opener.

Simulation process analysis

As illustrated in Figure 6a-b, the soil borrowing position of the furrow side pick-up blade is visually represented by setting the soil

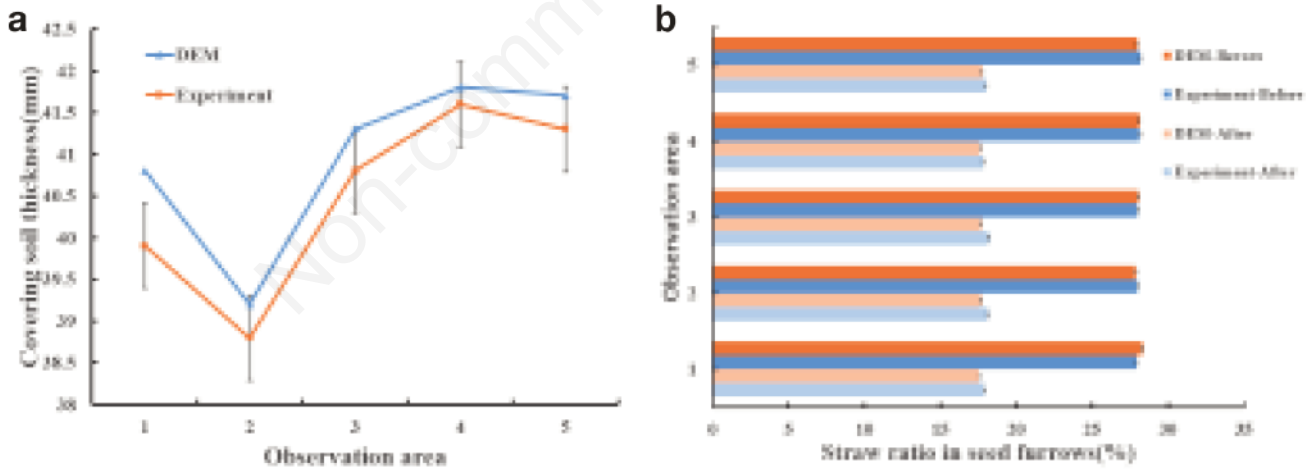

Figure 5. Comparison of discrete element simulation and indoor soil bin test for soil cover thickness and seed furrow straw ratio. **a)** Comparison of discrete element simulation of soil cover thickness and indoor soil bin test; **b)** comparison of discrete element simulation and indoor soil trough test for seed furrow straw ratio.

Table 4. Coding of experimental factors.

Factor level	Factor		
	Forward velocity v(km/h)	Endpoint tangent angle ω(°)	Angle of soil entry ε(°)
1	3	106	0
2	5	108	5
3	7	110	10

inside the seed furrow to orange, and the soil on the exterior of the seed furrow to khaki. By observing the change in color before and after the furrow side pick-up blade passes over the seed furrow, it can be determined that the blade extracts soil from both sides of the furrow, first covering the wheat seeds with khaki soil and then with orange soil from the seed furrow. This verifies the soil extraction position of the furrow side pick-up blade to be on the exterior of the seed furrow.

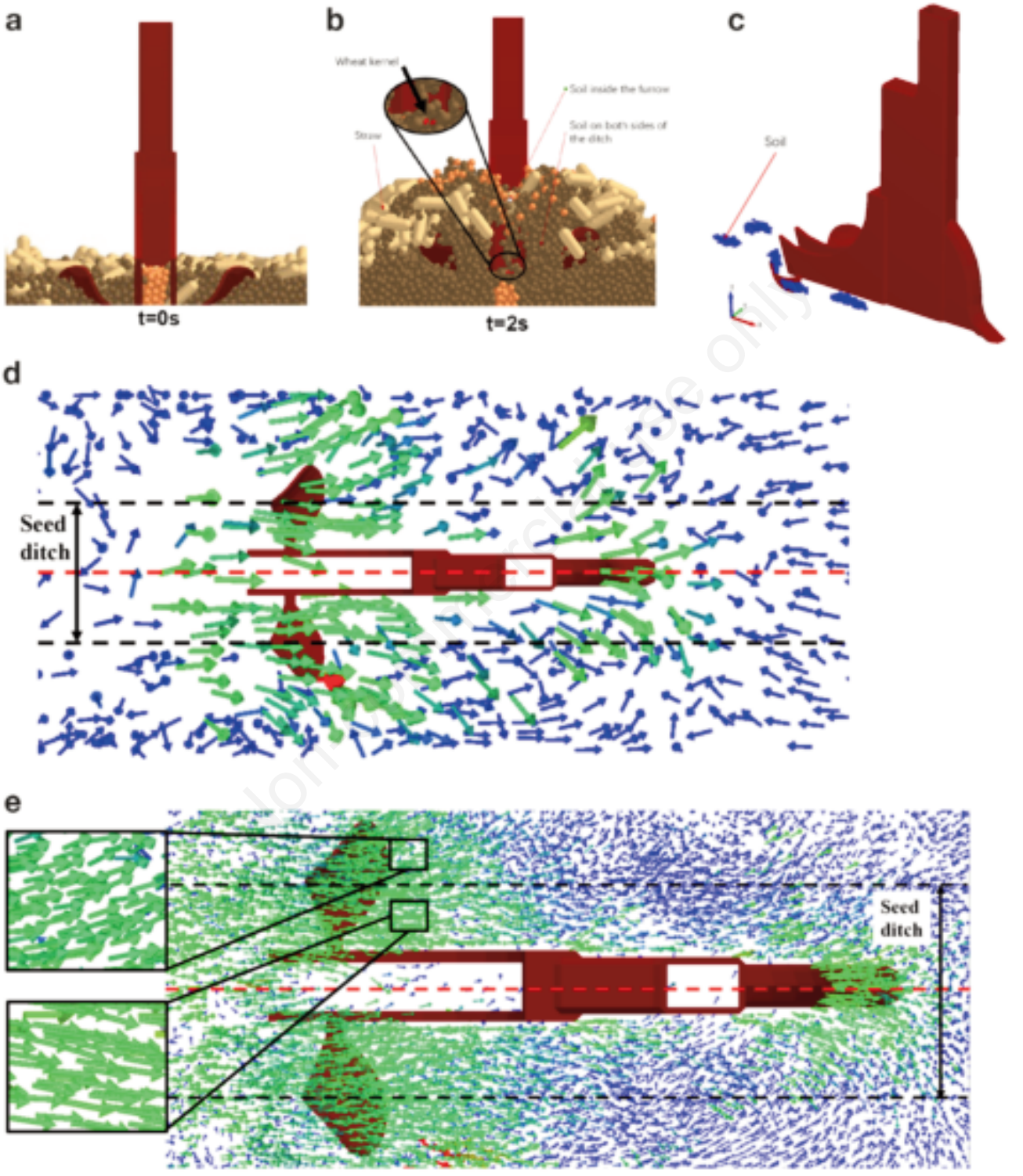

Figure 6. Analysis of simulation experiment process. **a**) Rear view of the opener through the soil at 0s; **b**) rear view of the opener through the soil at 2s; **c**) axonometric view of soil particle movement trend; **d**) vector diagram of the instantaneous velocity of straw particles (top view); **e**) vector diagram of the instantaneous velocity of soil particles (top view).

To investigate the movement pattern of soil particles as they pass through the furrow side pick-up blade, the particles on the side of the furrow adjacent to the opener were designated as blue for the purpose of observation. The movement trajectory of these selected soil particles is depicted in Figure 6c. As the furrow side pick-up blade passes through the blue soil particles on the furrow side, the particles are first lifted and then move in an upward, oblique direction along the curved surface. After reaching the highest point of the surface and being expelled, the soil particles begin to move towards the back of the opener due to inertia and then, under the influence of their gravity, exhibit a downward movement trend before finally falling into the seed furrow at the back of the opener. This motion law of the selected soil particles confirms the guiding effect of the surface of the furrow side pick-up blade on the soil on the furrow side, thereby demonstrating the design's feasibility.

In the EDEM simulation, the displacement and flow of particles as the opener moves through the furrow are represented by an instantaneous velocity vector diagram, where the magnitude of the particle velocity is indicated by its color. Figure 6d shows the vector diagram of the instantaneous velocity of the straw particles. It can be seen that the straw has two movement patterns after passing through the furrow side pick-up blade: it moves towards both sides of the seed furrow and falls into the seed furrow, or it continues to move forward with the furrow opener. From the comparison, it can be concluded that the proportion of straws moving to both sides of the seed furrow is relatively high at approximately 61.6%. The number of straws in the furrow is significantly reduced. Figure 6e shows the vector diagram of the instantaneous velocity of the soil particles. As can be seen from the enlarged image, the movement trends of the soil particles are similar to those of the straw particles, with roughly two movement patterns. Most of the soil particles move forward or into the furrow, which is approximately 68.4%. From this analysis it can be concluded that after the furrow-side pick-up blade operation, a larger number of straw particles accumulate on both sides of the seed furrow, while a significant proportion of the soil particles in the tillage layer on the furrow side accumulate inside the seed furrow, thus increasing the contact area between seed and soil in the furrow.

Trial protocol and results

The experimental program was executed through the EDEM software, and a total of 17 groups were conducted. The results of the measurements are presented in Table 5. A Box-Behnken test was applied to analyze the significance of the influence of the forward velocity (v) of the machine tool, the endpoint tangent angle (ω), and the angle of soil entry (ε) on the thickness of the cover soil and the proportion of straw in the seed furrow. The response model of the measurement index was obtained through regression equation fitting (Liu *et al.*, 2019). The simulation results were analyzed to identify the factors affecting the test indicators, and optimization of each combination was performed. Finally, a combination of test factors that were deemed more suitable was obtained.

Simulation results and analysis

The results in Table 5 were subjected to the significance and variance analysis using the Design-Expert software. A quadratic polynomial regression equation was selected and the stepwise regression method was employed to obtain the regression equation and perform the significance test.

Ansys of covering soil thickness

The concept of seed cover soil thickness refers to the thickness of the soil layer that covers the seeds, as depicted in Figure 7a. The test data were analyzed and fitted, and the results of the variance analysis of the cover soil thickness (H) are presented in Table 6.

It can be seen from Table 6 that X_2, X_3, X_2X_3, X_2^2, X_3^2 had highly significant effects on the covering soil thickness (H) ($p<0.01$); X_1, X_1^2, X_1X_2, X_1X_3 had significant effects on the covering soil thickness (H) ($0.01<p<0.05$). No factor was found to have a significant impact on the test index, which encompasses soil thickness (H) ($p>0.1$). The established regression model has a

Table 5. Test scheme and results.

No.	Forward velocity X_1 (Km/h)	Endpoint tangent angle X_2 (°)	Angle of soil entry X_3 (°)	Soil cover thickness H (mm)	Straw ratio in seed furrow (%)
1	7	108	10	41.331	23.509
2	7	110	5	41.919	23.574
3	5	108	5	41.556	21.941
4	5	106	10	31.247	22.448
5	5	106	0	33.769	22.597
6	5	108	5	43.890	21.833
7	5	110	10	40.889	22.506
8	3	110	5	33.487	22.549
9	5	108	5	42.060	21.258
10	7	106	5	33.770	22.536
11	3	108	0	35.990	23.583
12	5	108	5	40.155	21.246
13	5	110	0	32.271	23.325
14	5	108	5	42.869	21.386
15	3	106	5	33.639	22.571
16	7	108	0	33.641	23.845
17	3	108	10	36.528	22.971

P-value of less than 0.001, which demonstrates that the relationship between the dependent variable and all the independent variables in the model is highly significant. The P-value of 0.5203 for the lack of fit item is greater than 0.1, indicating that the lack of fit is not statistically significant. This result suggests that the regression model is an appropriate fit for the simulation test results. Therefore, the regression equation of the influence of each factor on the covering soil thickness H is obtained:

$$Y_1 = 42.11 + 1.38x_1 + 2.02x_2 + 1.79x_3 + 2.08x_1x_2 + 1.79x_1x_3 + 2.78x_2x_3 - 2.04x_1^2 - 4.37x_2^2 - 3.2x_3^2 \quad (8)$$

Analysis of the proportion of straw in seed furrows

The straw content in the seed furrow is indicative of the distribution of straw in the soil that covers the furrow, as depicted in Figure 7b. A statistical analysis was performed on the test data to determine the variability of the straw content in the seed furrow. The results of this analysis are presented in Table 7 through the use of variance analysis.

The results presented in Table 7 demonstrate that variables X_1^2 and X_3^2 have a highly significant effect ($p<0.01$) on the straw content in seed furrows. Meanwhile, variables X_1, X_2, and X_3 exhibit a significant effect ($0.01<p<0.05$) on the straw content. The remaining factors have no statistically significant impact ($p>0.1$) on the straw content in seed furrows as per the test index. The established regression model has a highly significant relationship ($p<0.001$) between the dependent variable and all independent variables. Additionally, the lack of fit, as indicated by the P-value of 0.9709 ($p>0.1$), is not statistically significant, implying that the regression model is a good fit for the simulation test results. Therefore, the regression equation of the influence of various fac-

Table 6. Variance analysis of covering soil thickness.

Parameter	Sum of squares	Degrees of freedom	Sum of mean squares	F	P
Model	289.8	9	32.2	17.19	0.0006**
X_1	15.17	1	15.17	8.1	0.0248*
X_2	32.57	1	32.57	17.39	0.0042**
X_3	25.65	1	25.65	13.69	0.0077**
X_1X_2	17.23	1	17.23	9.2	0.019*
X_1X_3	12.79	1	12.79	6.83	0.0348*
X_2X_3	31.02	1	31.02	16.56	0.0047**
X_1^2	17.47	1	17.47	9.33	0.0185*
X_2^2	80.24	1	80.24	42.84	0.0003**
X_3^2	43.03	1	43.03	22.97	0.002**
Residual	13.11	7	1.87		
Lack of fit	5.24	3	1.75	0.8864	0.5203
Pure error	7.88	4	1.97		
Cor total	302.91	16			

*significant ($p<0.05$); **very significant ($p<0.01$).

Table 7. VAnalysis of variance for the proportion of straw in various furrows.

Parameter	Sum of squares	Degrees of freedom	Sum of mean squares	F	P
Model	10.66	9	1.18	18.01	0.0005**
X_1	0.4465	1	0.4465	6.79	0.0351*
X_2	0.4522	1	0.4522	6.88	0.0343*
X_3	0.4589	1	0.4589	6.98	0.0333*
X_1X_2	0.2304	1	0.2304	3.5	0.1034
X_1X_3	0.019	1	0.019	0.2896	0.6071
X_2X_3	0.1122	1	0.1122	1.71	0.2327
X_1^2	4.24	1	4.24	64.53	<0.0001**
X_2^2	0.2545	1	0.2545	3.87	0.0898
X_3^2	3.72	1	3.72	56.63	0.0001**
Residual	0.4602	7	0.0657		
Lack of fit	0.0242	3	0.0081	0.0739	0.9709
Pure error	0.4361	4	0.109		
Cor total	11.12	16			

*significant ($p<0.05$); **very significant ($p<0.01$).

tors on the proportion of straw in the seed furrow is obtained:

$$Y_2 = 21.53 + 0.2363x_1 + 0.2377x_2 - 0.2395x_3 + 0.24x_1x_2 + 0.069x_1x_3 - 0.1675x_2x_3 + x_1^2 + 0.2459x_2^2 + 0.9403x_3^2 \quad (9)$$

Response surface analysis

The response surface is a graphical representation of the relationship between two interacting experimental factors and the response value when all other factors are held constant. The degree of influence of the two experimental factors on the response value is evaluated based on its slope. Through data processing using the Design-Expert software, the response surface for the significant and relatively significant interactions between the forward velocity (X_1), the endpoint tangent angle (X_2), and the angle of soil entry (X_3) on the cover soil thickness (H) and the proportion of straw in the seed furrow was derived, as demonstrated in Figure 8a-b.

Figure 8a depicts the interaction between the forward velocity, the endpoint tangent angle, and the angle of soil entry on the overburden thickness. It is evident that each factor has a significant impact on the soil cover thickness.

As shown in Figure 8a, when the forward velocity is kept constant, the soil cover thickness initially increases and then decreases with an increase in the endpoint tangent angle. The optimal endpoint tangent angle range is 107.8° to 109.5°. Similarly, when the endpoint tangent angle is held constant, the soil cover thickness increases initially and then decreases with an increase in the forward velocity, with an optimal forward velocity range of 4.7 km/h to 6.8 km/h. When the forward velocity is at its lowest and the endpoint tangent angle is at its highest, the soil cover thickness is at its minimum. The slope of the forward velocity is steeper than that of the endpoint tangent angle, indicating that the effect of the forward velocity is more significant.

As depicted in Figure 8a2, the relationship between the forward velocity, the endpoint tangent angle, and the angle of soil entry on overburden thickness is further explored. When the forward velocity is kept constant, the soil cover thickness first increases and then decreases with the increase of the angle of soil entry, with the optimal range of the angle of soil entry being 4.8° to 9.0°. On the other hand, when the angle of soil entry is constant, the soil cover thickness increases initially and then decreases with an increase in forward velocity, and the optimal range of the for-

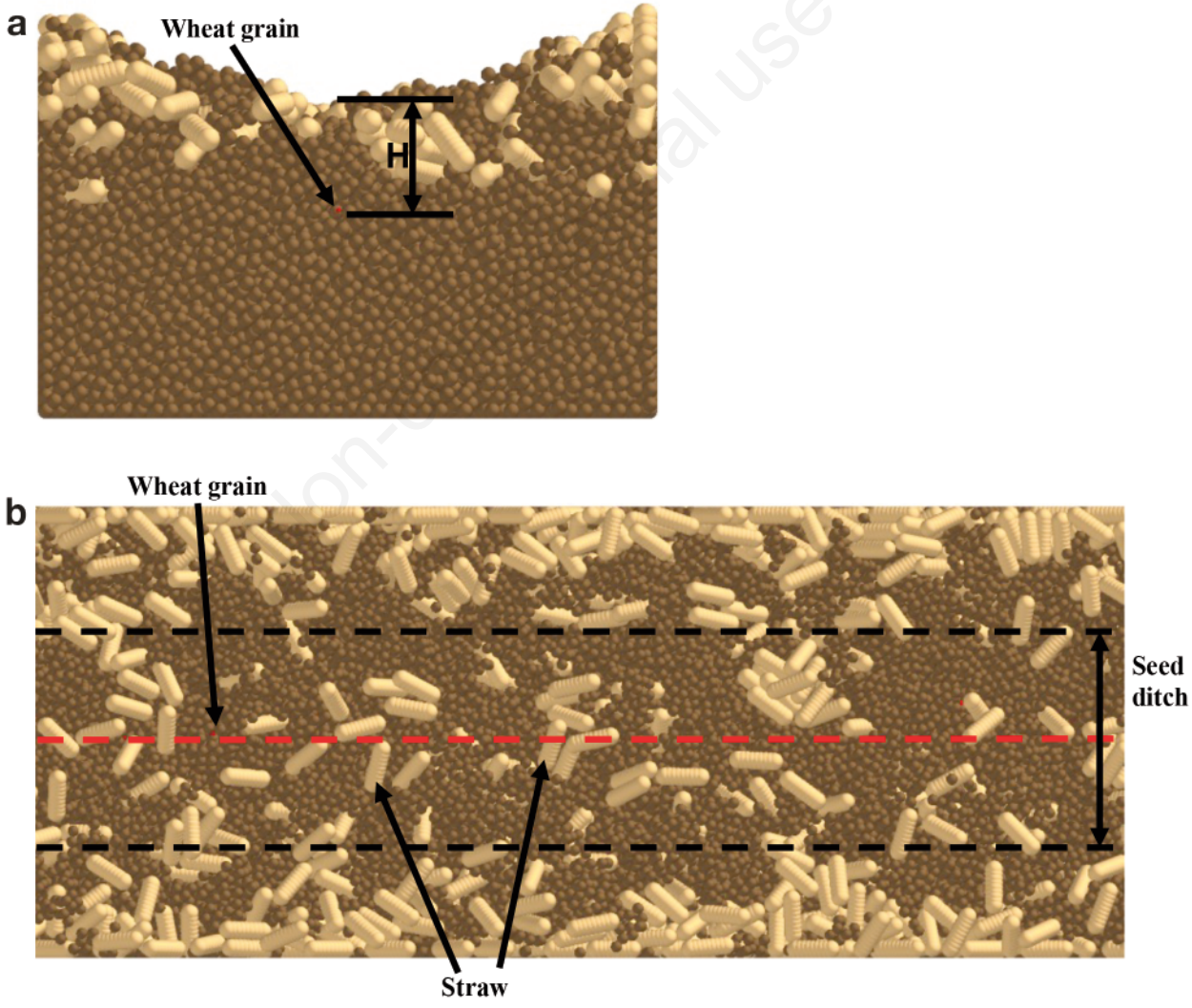

Figure 7. Simulation experiment results. **a**) Schematic diagram of covering soil thickness; **b**) distribution map of straw in various furrows.

ward velocity is found to be 5.1 km/h to 6.3 km/h. As the angle of soil entry decreases and the forward velocity increases, the soil cover thickness reaches its minimum. The slope of the forward velocity is steeper than that of the angle of soil entry, indicating a more significant effect of the forward velocity on the soil cover thickness. Furthermore, Figure 8a3 provides insight into the relationship between the endpoint tangent angle and the angle of soil entry on overburden thickness. When the endpoint tangent angle is held constant, the soil cover thickness first increases and then decreases with the increase of the angle of soil entry, with the optimal range of the angle of soil entry being 5.0° to 9.3°. When the angle of soil entry is kept constant, the soil cover thickness increases initially and then decreases with the increase in endpoint tangent angle, and the optimal range of the endpoint tangent angle is found to be 108.2° to 109.4°. The soil cover thickness reaches its minimum when the endpoint tangent angle is the smallest and the angle of soil entry is the largest. As depicted in Figure 8b, the interaction between various factors, including the forward velocity, endpoint tangent angle, and angle of soil entry, on the ratio of seed furrow straw is presented. With regards to Figure 8b1, when the forward velocity is held constant, the proportion of straw in the seed furrow first decreases and then increases with an increase in the endpoint tangent angle. The optimal endpoint tangent angle range, in this case, lies between 106.4° and 108.3°. When the endpoint tangent angle is held constant, the proportion of straw in the seed furrow decreases first and then increases with the increase in forward velocity, and the optimal forward velocity range is 4.4 km/h to 5.2 km/h. The proportion of straw in the seed furrow is found to be the smallest when both the forward velocity and the endpoint tangent angle take the middle value. The influence of the endpoint tangent angle is found to be more significant as the slope of the endpoint tangent angle is steeper as compared to the forward velocity.

Similarly, as shown in Figure 8b2, when the forward velocity is held constant, the proportion of straw in the seed furrow decreases first and then increases with the increase in the angle of soil entry. The optimal range of the angle of soil entry, in this case, is 4.4° to 7.2°. When the angle of soil entry is held constant, the proportion of straw in the seed furrow decreases first and then increases with an increase in forward velocity, and the optimal forward velocity range is 4.1 km/h to 5.2 km/h. The proportion of straw in the seed furrow is found to be the smallest when both the angle of soil entry and the forward velocity take the middle value, and the impact of forward velocity is found to be more significant as the slope of the forward velocity is steeper as compared to the angle of soil entry. Lastly, as depicted in Figure 8b3, when the endpoint tangent angle is held constant, the proportion of straw in the seed fur-

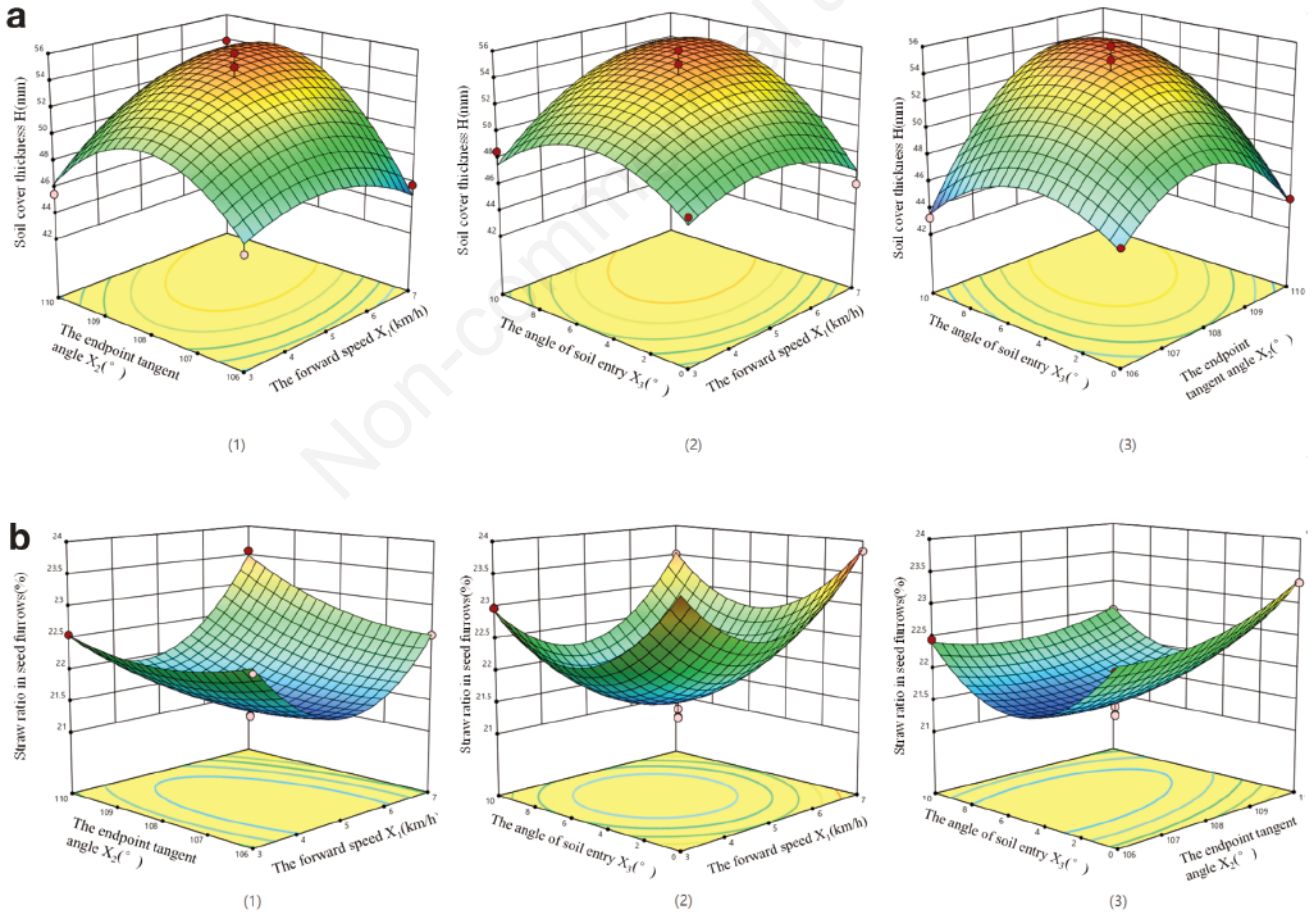

Figure 8. Response surface. **a**) The influence of test factors on the thickness of the covering soil; **b**) the experimental factors affecting the proportion of straw in seed furrows.

row decreases first and then increases with an increase in the angle of soil entry, and the optimal range of the angle of soil entry is 4.2° to 6.6°. When the angle of soil entry is held constant, the proportion of straw in the seed furrow decreases first and then increases with an increase in the endpoint tangent angle, and the optimal endpoint tangent angle range is 106.4° to 107.8°. The proportion of straw in the seed furrow is found to be the smallest when the endpoint tangent angle takes the smaller value and the angle of soil entry takes the middle value, and the influence of the endpoint tangent angle is found to be more significant as the slope of the endpoint tangent angle is steeper as compared to the angle of soil entry. In this study, the optimization of the combination of test factor levels was performed through the analysis of six response surfaces using Design-Expert software. Based on agronomic requirements and simulation experiments, it was determined that the optimal soil stress value is achieved when the straw content in the soil is within the range of 10% to 30%. Thus, in this study, the lowest straw content was established as the optimization target, and the optimal constraint condition was set as a covering soil thickness of no greater than 40mm. Among the multiple sets of optimized parameter combinations obtained, a set of optimal parameters was selected, which included a forward velocity of 4.86 km/h, an endpoint tangent angle of 107.17°, and an angle of soil entry of 5.46°. These parameters were determined to result in the ideal performance of the furrow side pick-up blade. It was predicted that the covering soil thickness would be 40 mm, with a proportion of straw in the seed furrow of 21.46%.

Conclusions

First, the interaction model of soil-straw- the furrow side pick-up blade established through the DEM offers a viable technical solution for addressing the seed-soil contact problem under straw cover. Among the factors affecting the proportion of straw in the furrow, forward velocity, Endpoint tangent angle, and angle of soil entry exhibit significant effects, with the square terms of forward velocity and angle of soil entry demonstrating highly significant impacts. Other factors do not significantly affect the experimental indicator, the proportion of straw in the furrow.

Through response surface analysis, we have determined the extent of the influence of forward velocity, Endpoint tangent angle, and angle of soil entry on burial depth and the proportion of straw in the furrow.

Finally, the optimal operational parameter combination consists of a forward velocity of 4.86 km/h, an Endpoint tangent angle of 107.17°, and angle of soil entry of 5.46°. Under these conditions, the soil exhibits the lowest straw content, a burial depth of 40 mm, and a proportion of straw in the furrow of 21.46%.

These findings provide crucial guidance for understanding the interactions between agricultural machinery components, straw, and soil, offering valuable insights for practical field operations. In future research and real-world applications, these conclusions can inform the selection of optimal operating parameters to enhance the performance and efficiency of agricultural machinery. This study provides robust support for addressing critical issues in field operations and holds significant relevance for the sustainable development of modern agriculture.

References

Aikins K.A., Barr J., Ucgul M., Jensen T., Antille D.L., Desbiolles J.M.A. 2020. No-tillage furrow opener performance: A review of tool geometry, settings and interactions with soil and crop residue. Soil Res. 58:603-21.

Bai L., Huang Y., Gao P., Ding S., Zhang H., Fu Z., Zhu R. 2020. Design and test of seed and fertilizer separate device based on double disc covering soil. J. Northwest A & F University (Natural Science Edition). 1:135-45+154.

Barker M.E., Plouffe C. 2017. Simulation of Planter Row Cleaner in Corn Residue Using Discrete Element Modeling. ASABE Annual International Meeting (p. 1).

Chandio F.A. 2013. Interaction of straw-soil-disc tool under controlled conditions. Unpublished thesis (PhD), of Nanjing Agricultural University, China.

Chen H., Hou L., Hou S., Li Y., Min S., Chai Y. 2018. Design and Optimization Experiment of Anti-blocking Mechanism of No-tillage Planter for Grand Ridge with Raw Corn Stubble. Trans. Chin. Soc. Agric. Machin. 8:59-67.

Ding Q., Ren J., Belal E.A., Zhao J., Ge S., Li Y. 2017. DEM Analysis of Subsoiling Process in Wet Clayey Paddy Soil. Trans. Chin. Soc. Agric. Machin. 3:38-48.

Fu S.Y., Feng X.Q., Lauke B., Mai Y.W. 2008. Effects of particle size, particle/matrix interface adhesion and particle loading on mechanical properties of particulate–polymer composites. Compos. B. Eng. 39:933-61.

Gu F., Hu Z., Chen Y., Wu F. 2016. Development and experiment of peanut no-till planter under full wheat straw mulching based on "clean area planting". Trans. Chin. Soc. Agric. Eng. 20:15-23.

Itasca C.G.I. 2005. PFC3D (Particle Flow Code in Three Dimensions). Minneapolis, Minnesota, USA.

Liu F., Jian Z., Chen J. 2018a. Modeling of flexible wheat straw by discrete element method and its parameter calibration. Int. J. Agric. Biol. Eng. 11:42-6.

Liu J., Wang H., Wang Q., Li S., Li H., He J. 2018b. Design and experiment of strip cleaning device of no and minimum-tillage corn seeder. Transact. CSAM. 49:132-40.

Liu F., Zhang J., Li B., Chen J. 2016. Calibration of parameters of wheat required in Discrete Element Method simulation based on repose angle of particle heap. Trans. Chin. Soc. Agric. Eng. 12:247-53.

Liu X., Zhang Q., Liu L., Wei G., Xiao W., Liao Q. 2019. Surface Optimization of Ship Type Ditching System Based on Differential Geometry and EDEM Simulation. Trans. Chin. Soc. Agric. Machin. 8:59-69.

Lu H., Feng Y., Gao Q., Xing J., Chen Y., Yang L., Xue L. 2020. Surface soil mixing is more beneficial than the plough layer mixing mode of biochar application for nitrogen retention in a paddy system. Sci. Total Environ. 718:137399.

Lv J., Liu Q., Li Z., Li J., Liu Z. 2021. Design and Experiment of Soil Cultivating Device of Plowshare Potato Field Cultivator. Trans. Chin. Soc. Agric. Machin. 7:71-82.

Niu Q., Wang Q., Chen L., Li H., He J., Li W. 2017. Design and experiment on straw post-covering wheat planter. Trans. Chin. Soc. Agric. Machin. 48:52-9.

Shi L., Zhao W., Sun W. 2017. Parameter calibration of soil particles contact model of farmland soil in northwest arid region based on discrete element method. Trans. Chin. Soc. Agric. Eng. 33:181-7.

Sun K., Yu J., Liang L., Wang Y., Yan D., Zhou L., Yu Y. 2022. A DEM-based general modelling method and experimental veri-

fication for wheat seeds. Powder Technol. 401:117353.
Sun L., Gibson R.F., Gordaninejad F., Suhr J. 2009. Energy absorption capability of nanocomposites: a review. Compos. Sci. Technol. 69:2392-409.
Wang X., Hu H., Wang Q., Li H., He J., Chen W. 2017. Calibration Method of Soil Contact Characteristic Parameters Based on DEM Theory. Trans. Chin. Soc. Agric. Machin. 12:78-85.
Wei G., Zhang Q., Liu L., Xiao W., Sun W., Liao Q. 2020. Design and Experiment of Plowing and Rotary Tillage Buckle Device for Rapeseed Direct Seeder. Trans. Chin. Soc. Agric. Machin. 6:38-46.
Wu T., Huang W., Chen X., Ma X., Han Z., Pan T. 2017. Calibration of discrete element model parameters for cohesive soil considering the cohesion between particles. J. South Chin. Agric. Univ. 38:93-8.
Xiong P., Yang Z., Sun Z., Zhang Q., Huang Y., Zhang Z. 2018. Simulation analysis and experiment for three-axis working resistances of rotary blade based on discrete element method. Trans. Chin. Soc. Agric. Eng. 18:113-21.
Yu J., Lu C., Wei R., Fu X., Li K., Tang Z., Wang F. 2018. Simulation test of performance of wheat precision seed-metering device based on Discrete Element Method. Jiangsu Agric. Sci. 8:225-8.
Zhai L. 2011. Study on the effects of plough's working and structure parameters on its resistance under rheological soil conditions. PH.D. Nanjing Agric. Univ. Chin.
Zhang K., Huang J., Yang M., Zhang F., Huang X., Zhao C. 2010. Finite element analysis and experimental verification of wheat grain under compression loads. Trans. Chin. Soc. Agric. Eng. 6:352-6+391.
Zhang R., Li J., Li Y., Liu Z., Chen B. 2009. DEM macroscopic and mesoscopic analysis in disturbed behavior of soil acted by part with complex surface. J. Jilin Univ. Eng. Technol. Ed. 5:1218-23.
Zhang T., Liu F., Zhao M., Ma Q., Wang W., Fan Q., Yan P. 2018. Determination of corn stalk contact parameters and calibration of Discrete Element Method simulation. J. Chin. Agric. Univ. 4:120-7.
Zhang Z., He J., Li H., Wang Q., Ju J., Yan X. 2017. Design and Experiment on Straw Chopper Cum Spreader with Adjustable Spreading Device. Trans. Chin. Soc. Agric. Machin. 9:76-87.
Zhao H., He J., Li H., Liu C., Zheng K., Zhang Z. 2018a. Design and Experiment of Strip Rotary-cut-throw Anti-blocking Implement. Trans. Chin. Soc. Agric. Machin. 5:65-75.
Zhao H., He J., Li H., Mao Y., Liu P. 2018b. Comparison on soil, straw disturbance, and resistance of conventional and plain-straight blade for strip-tillage with Discrete Element Method. Int. Agric. Eng. J. 27:229-40.
Zhao L., Zhang Z., Wang C., Jian S., Liu T., Cui D., Ding X. 2018c. Design of monitoring system for wheat precision seeding-fertilizing machine based on variable distance photoelectric sensor. Trans. Chin. Soc. Agric. Eng. 13:27-34.
Zhao H., He J., Zheng Z., Zhang Z., Liu W. 2020. Strip Tillage Inter-row Residue Side-throwing Device of No/minimum-till Seeder for Anti-blocking and Seedbed-cleaning. Trans. Chin. Soc. Agric. Machin. 12:24-34.
Zhao S., Liu H., Yang C., Yang L., Gao L., Yang Y. 2021. Design and Discrete Element Simulation of Interactive Layered Subsoiler with Maize Straw Returned to Filed. Trans. Chin. Soc. Agric. Machin. 3:75-87.
Zhao S., Wang J., Yang C., Chen J., Yang, Y. 2019. Design and Experiment of Stubble Chopper under Conservation Tillage. Trans. Chin. Soc. Agric. Machin. 9:57-68.
Zhong X., Zhang X., Geng Y., Wei Z., Cheng X., Wang X. 2023. Research on Load Transfer of Straw-soil Complex Based on Discrete Element Method. J. Agric. Mechan. Res. 3:17-24.

spreading machine to return the straw to the field. During the operation process, the straw is finely crushed, and the information parameters such as the position, width, uniformity, and distance of the thrown straw are controlled and adjusted to regulate the straw cover state. Realize to clean the straw on the ground before planting to reduce the impact of the straw cover on planting. Liu *et al*. (2018b) designed a stubble cleaning device with a seed belt cleaning curved knife as the main working part to solve the problems of serious mixing of soil and straw, high seed drying rate, and poor sowing quality when sowing corn by strip rotary tillage. The field test verified that the machine passed well, the soil disturbance was low, and the cleanliness of the seed belt could reach more than 80%. Zhao *et al*. (2018a) developed a strip-type tillage and back-throwing anti-blocking device, which throws the straw between the seed rows during the crushing process, reducing the accumulation of straw in the seed bed area. Niu *et al*. (2017) designed a post-straw mulching wheat planter for sowing wheat on corn straw mulched land prone to clogging and seed drying, which can complete rotary tillage, seeding, soil covering, straw covering, suppression, and other processes once in the field. Based on the analysis of rototiller throwing and straw throwing movement, the structure and position parameters of the soil guide were determined, and the straw-soil sequential mulching was realized.

The aim of this study is to improve seed-soil contact and develop a furrow side pickup blade based on a chisel-type furrow opener for strip-tillage of wheat in the double-cropping area of wheat and corn in Huanghuaihai. By using the Discrete Element Method (DEM), we established a model for the interaction between soil, straw, and a furrow side pickup blade. This model allowed us to determine the optimal working parameters for the furrow side pickup blade. It provides a feasible technical solution for addressing the issue of seed-soil contact under straw cover.

Materials and Methods

Overall structure and working principle

The overall structure of the chisel opener furrow side pick-up blade is shown schematically in Figure 1. The main components of the system include the opener blade tip, the opener handles, and the curved surface of the furrow side pick-up blade. The latter is securely welded to both sides of the opener, ensuring the structural integrity and stability of the system.

During the tilling operation, the front end of the furrow side pick-up blade engages the soil level at a specific angle of soil entry. As the opener progresses, the soil located on both sides of the seed furrow is lifted along the curved surface of the furrow side pick-up blade, with the latter gradually inwardly curving front to back. The soil, after being turned over, rises to a certain height, at which point the curved surface exerts an inward extrusion effect upon the soil, resulting in a continuous turnover of the soil in contact with and adjacent to it. This culminates in the process of collecting and covering the wet soil from the side of the furrow.

The furrow side pick-up blade surface design

In this study, the horizontal element straight-line method was employed, which conceptualizes the surface of the plow body as a continuous surface constituted by horizontal element straight lines moving upward along a guide curve from the bottom surface. The length of this horizontal element straight line and the angle θ between them and the x-axis vary as the guide curve ascends (Lu *et al.*, 2020; Wei *et al.*, 2020). The surface of the plow body was constructed by the movement of the horizontal element straight lines along a horizontal trace, as illustrated in Figure 2a.

A Guide Curve Model was established, as depicted in Figure 2b. The determination of its shape is a crucial aspect of the design of the furrow side pick-up blade surface and is influenced by various factors, including the height of the curve (h), the opening (L), the starting angle (ε), the endpoint tangent angle (ω), and the length of the starting straight-line segment (s).

The determination of the height of the guide curve (h), representing the depth of cultivation, is a crucial aspect of the design of the furrow side pick-up blade surface. In this study, the height of the highest point of the surface was set to 50mm. The ploughing width (L), which represents the opening of the blade, was determined to be 90mm based on practical experience. The soil draft angle (ε) plays a critical role in the design of the furrow side pick-up blade surface. A larger soil draft angle leads to a shorter soil extraction blade and greater tillage resistance. Based on empirical evidence, the soil draft angle was set to 25°, with a range of 20-30°. Furthermore, the endpoint tangent angle (ω) also influences the performance of the furrow side pick-up blade. A larger endpoint tangent angle results in greater wing twists and improved soil-turning effects. The endpoint tangent angle is determined by the inclination angle (Δε) at the end of the guide curve and the starting angle (ε), as described by the following formula:

$$\omega = \frac{\pi}{2} + \varepsilon - \Delta\varepsilon \quad (1)$$

According to the design specifications outlined in the "Agricultural Machinery Design Manual" the range of the derivative curve, Δε, is typically between 0° and 10°. As such, the angular velocity, ω, which serves as a key experimental variable, is set to values ranging from 106° to 110°.

The variation of the element line angle, θ, is illustrated in Figure 2c. The variation law of θ displays two distinctive segments, exhibiting a trend of first decreasing and then increasing. The initial segment is linear, with its starting point represented by θ_0, which generally falls within the range of 35° to 40°. The minimum value of the element line angle, θ_{min}, can be calculated as θ_0-(2° to 4°), with a sample value of 38°. The second segment is curved, for which a parabolic function has been chosen to model the soil turning surface. The curve function is expressed as $\theta_{max}=\theta_0+(7°$ to $15°)$, with a sample value of 50°.

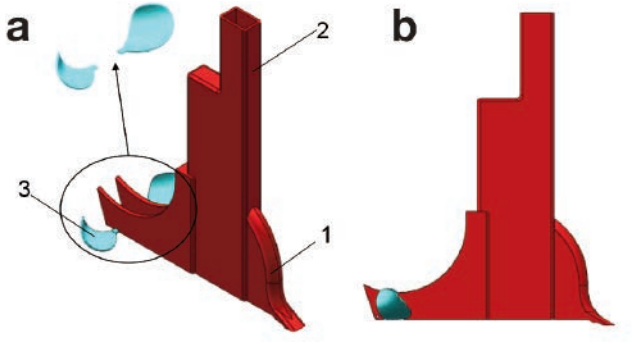

Figure 1. Schematic diagram of the overall structure: **a**) the overall structure; **b**) side view; 1) opener blade tip; 2) opener handle; 3) the furrow side pick-up blade curved surface.

Force analysis of the angle of soil entry

The soil extraction section of the soil covering operation requires precise guidance at the outset to ensure that the cut soil can effectively leap up and lift the moist soil from the furrow bottom to the surface, while simultaneously facilitating the accumulation of a substantial amount of soil. The front end of the furrow side pick-up blade undergoes a force analysis, as depicted in Figure 2d.

In Figure 2d, N_0 represents the positive pressure reaction force exerted on the front section of the furrow side pick-up blade, T_0 denotes the friction force acting on the working surface, R_0 represents the resultant force generated by the combination of N_0 and T_0, φ represents the friction angle, F_0 represents the forward direction component force of N_0, ε_0 represents the angle of soil entry and the angle of soil entry clearance, and β represents the angle of soil clearance. When the opener moves at a constant velocity, the forward direction component force F_0 of the soil access portion's positive pressure N_0 remains constant and is equal to the soil resistance of the furrow side pick-up blade at a specific depth. As a result, the working surface's force R_0 can be indirectly estimated through the combined force of surface positive pressure N_0 and frictional force T_0 (Lv *et al.*, 2021).

The vertical component R_{0Z} of the soil reaction force in the front section of the furrow side pick-up blade is:

$$R_{0z} = F_0 \sin\varepsilon_0 \cos\varepsilon_0 - F_0 \sin\varepsilon_0 \tan\varphi \sin\varepsilon_0 = F_0\left[\frac{\sin(2\varepsilon_0)}{2} - \sin^2(\varepsilon_0)\tan\varphi\right] \quad (2)$$

The component R_{0X} of the soil reaction force in the front section of the furrow side pick-up blade in the horizontal direction is:

$$R_{0X} = F_0 \sin\varepsilon_0 \sin\varepsilon_0 + F_0 \sin\varepsilon_0 \tan\varphi \cos\varepsilon_0 = F_0\left[\sin^2(\varepsilon_0) + \frac{\sin(2\varepsilon_0)}{2}\tan\varphi\right] \quad (3)$$

In the formula ε_0, the angle of soil entry and the angle of soil entry clearance (°).

For the furrow side pick-up blade, reducing the horizontal component of the soil reaction force on its front section can effectively improve the soil entry performance of the tool, so the above formula is derived:

$$R'_{0X} = \sin(2\varepsilon_0) + \cos(2\varepsilon_0)\tan\varphi \quad (4)$$

Since φ is the friction angle, that is, tan φ is a fixed value, the smaller the value of ε_0, the better. Therefore, the angle of soil entry clearance β is selected as one of the test factors, and its value ranges from 0° to 10°.

Surface force analysis

In the soil extraction process, the turning of soil is the main operation, and based on this effect, the stress situation of the soil during the turning process is analyzed utilizing the three-sided wedge simplification principle as depicted in Figure 2e1. The assumption is made that the three-sided wedge moves at a constant velocity in the positive direction of the x-axis. In Figure 2e1, α represents the soil starting angle, β represents the soil turning angle, γ represents the bulldozing angle, and point m is taken on the surface. The primary forces at point m include the soil pressure N and the total friction force T between the soil and the wedge surface, and R is the resultant of N and T. When the wedge surface moves

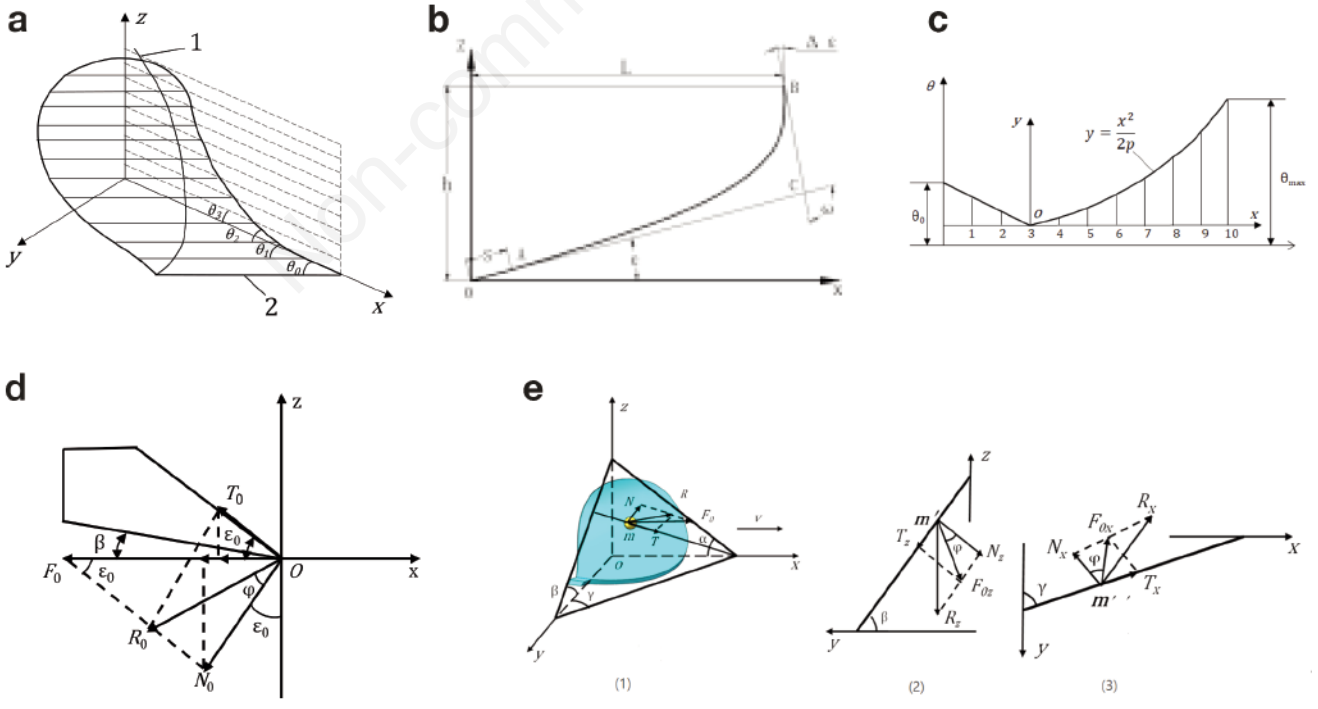

Figure 2. Theoretical analysis: **a**) the furrow side pick-up blade; 1) the guide curve; 2) the horizontal element straight line; **b**) model of guide curve of the furrow side pick-up blade surface; **c**) variation curve of line angle of the furrow side pick-up blade surface element; **d**) force analysis of the front end of the furrow side pick-up blade; **e**) force analysis on the surface of the furrow side pick-up blade.

at a constant velocity, the soil resistance in the horizontal direction on the wedge surface is equivalent to the forward component force F_0 of the positive pressure. Utilizing the analysis principle of the soil entry angle, the soil resistance F_0 can be employed to symbolize the force on the wedge surface (Zhai, 2011).

In Figure 2e2, the projection of the force at point m onto the yoz plane results in the force at point m' in the vertical section. The force at point m' can be represented by the following equation:

$$\begin{cases} N_z = R_z cos\beta = F_0(\frac{sin(2\alpha)}{2} - sin^2\alpha tan\varphi)cos\beta \\ T_z = R_z cos\beta tan\varphi = F_0(\frac{sin(2\alpha)}{2} - sin^2\alpha tan\varphi)cos\beta tan\varphi \end{cases} \quad (5)$$

In the formula: β is yoz face wedge angle, that is, turning the soil angle, (°); N_Z is yoz dihedral wedge pressure, (N); T_Z is yoz dihedral wedge friction, (N).

Projecting the above two-component force to the xoy plane, as shown in Figure 2e3, the soil reaction force of m'' on the horizontal plane can be obtained as:

$$R_l = F_0(\frac{sin(2\alpha)}{2} - sin^2\alpha tan\varphi)(cos^2\gamma + \frac{sin\,(2\gamma)}{2} tan\varphi) \quad (6)$$

In the formula γ is xoy face wedge angle, that is, the bulldozer angle, (°)

Simulation test

Soil model calibration

Fu (2008) and Sun (2009) found in their research that the smaller the particle radius, the smaller the error of the simulation experiment and physical experiment, but the calculation time will be doubled. The larger the particle radius, the faster the stress propagation between particles. After comprehensive consideration, soil particles with a particle radius of 5mm were selected with reference to Shi *et al.* (2017) on the premise of ensuring accuracy. The parameters of the soil particle model were mainly obtained with reference to the literature of the same soil type (Ding *et al.*, 2017; Wang *et al.*, 2017; Xiong *et al.*, 2018; Zhang *et al.*, 2009; Zhao *et al.*, 2019). The choice of contacting model has a great impact on the accuracy of soil discrete element simulation results. Wu *et al.* (2017) have proved that the Hertz-Mindlin with Johnson-Kendall-Roberts contact model is better than the traditional Hertz contact model. The model comprehensively considers the elastic deformation of soil particles and adds the influence of the cohesive force of the interaction between particles based on Hertz's theory. The value of the main parameter in the model, surface energy, is related to the amount of bond strength, which in turn determines the degree of soil fragmentation of the opener during tillage. In this paper, a soil accumulation angle test was adopted to verify the parameters under the condition of 15.8% soil moisture content. The simulation parameters of the model are shown in Table 1.

The soil accumulation angle test is composed of funnel, bracket, and receiving plate. The bottom of the funnel is 300mm away from the receiving plate. During the test, the lower end of the funnel is close to a thin plate, and the soil samples to be tested are evenly distributed into the funnel, followed by rapid withdrawal of the thin plate. The soil naturally falls from the funnel to the receiving plate under the action of gravity, and when the soil accumulation shape is stable, the digital display angle ruler is used to measure the soil accumulation angle from three directions. The above test is repeated five times, and the arithmetic average of the accumulated angle five times is taken as the final test result, the size of which is 38.5°, as shown in Figure 3a. The funnel model of actual size was established and imported into EDEM (Altair Engineering, Troy, MI, USA). The receiving plate was placed at the bottom of the funnel, and the relative position between the two was adjusted to be consistent with the real situation. Waiting for the particles to move in the catch plate until all the particles are relatively stable and form a stable pile of particles for post-processing, the measurement result is 38.8°, as shown in Figure 3b.

Modelling the straw structure

In the construction of the discrete element model for straw, multiple spherical surfaces of varying sizes and positions are established to form a strip model that closely resembles corn straw. This is achieved through stacking the spherical surfaces, with a 50% overlap between adjacent spheres serving as a compromise between surface resolution and computational efficiency. Referring to the method of selecting straw models in Itasca (2005), Chandio (2013), and Barker and Plouffe (2017), the furrow side pick-up blade designed in this paper pushes rather than cuts the straw, so the straw is also established as rigid. In this study, 20 corn stalks were randomly selected from the field of measurement and calculation. The discrete element model was constructed with 9 particles with a radius of 8mm and a length of 48 mm per stalk, and a total of 1843 corn stalks were randomly distributed in the topsoil layer. The Hertz-Mindlin (no slip) contact model was used to model the mechanical relationship between straw particles, based on the properties of crushed corn stalks returned to the field (Zhong *et al.* 2023). The parameters for the straw were obtained from relevant references (Zhao *et al.*, 2021; Zhang *et al.*, 2018; Yu *et al.*, 2018) and are shown in Table 2. The straw particle model is shown in Figure 3c.

Table 1. Soil particle parameters.

Parameter	Value
Soil solids density of particles ρ/(kg·m^{-3})	1680
Soil particle bonding radius r/mm	5.67
Soil shear modulus G/MPa	1
Poisson's ratio: soil ν	0.3
Coefficient of restitution soil-soil e	0.56
Coefficient of static friction soil-soil μ_s	0.79
Coefficient of rolling friction soil-soil μ_r	0.22
Soil JKR surface energy/(J·m^{-2})	8.06

JKR; Johnson-Kendall-Roberts contact model.

Table 2. Parameters of straw particles.

Parameter	Value
Straw solids density of particles ρ/(kg·m^{-3})	241
Poisson's ratio: straw ν	0.4
Straw shear modulus G/MPa	1
Coefficient of restitution straw-soil e	0.6
Coefficient of static friction straw-soil μ_s	0.537
Coefficient of rolling friction straw-soil μ_r	0.16
Coefficient of restitution straw-straw e	0.485
Coefficient of static friction straw-straw μ_s	0.213
Coefficient of rolling friction straw-straw μ_r	0.098

Modelling the wheat grain structure

In this study, the wheat grain model was established using Jimai 22. 100 full, undamaged, and pest-free wheat grains were randomly selected, and their triaxial diameter was measured using a vernier caliper, with the average value taken as the representative size (Liu *et al.*, 2016). The average geometric size of the wheat grains was found to be 5.1 mm in length, 2.8 mm in width, and 3.8mm in height. Since the surface of the wheat grains was smooth and fluid, it was assumed to be a uniform linear elastic material with homogeneous properties. The multi-sphere method was adopted to construct a double ellipsoid model of the wheat grain, as it was found to describe the actual wheat grains more accurately, based on the research of Sun *et al*. (2022) and Zhang *et al*. (2010). The wheat grain was simplified into 5 ball-bonded combined grains, piled up by 5 grains with different radii, with a total length of 5mm, as shown in Figure 3d-e. As the wheat grains are approximately ellipsoidal and exhibit no adhesion force on their surface, the Hertz-Mindlin (no-slip) non-slip contact model was selected as the material movement contact model. Other parameters of the grains were obtained by referencing relevant literature (Zhao *et al.*, 2018c; Liu *et al.*, 2018a), as shown in Table 3.

Discrete element modeling

In the simulation experiment, a virtual test soil bin was established with dimensions of 2000 mm in length, 1000 mm in width, and 200mm in depth. The choice of a 2000 mm length for the soil bin serves to stabilize the movement of the opener and provide sufficient data collection length. The 1000 mm width accommodates sufficient lateral particle movement to prevent excessive particles from flowing back into the seed furrow. The 200 mm depth allows for a tillage depth of 50mm with an adequate margin below to simulate actual soil conditions. To ensure the validity of the simulation, soil particles in the tillage layer and straws were generated randomly. During the simulation, a grain factory for wheat grains was established at the rear end of the opener and generated a total of 300 wheat grains through the interaction of the opener movement and the grain factory (Bai *et al.*, 2020). For the simulation experiment, the forward speed of the opener was set to 5 km/h, the endpoint tangent angle was set to 108°, and the soil entry angle was set to 5°.

Table 3. Wheat grain parameters.

Parameter	Value
Grain solids density of particles ρ/(kg·m^{-3})	1373
Poisson's ratio: soil ν	0.42
Grain shear modulus G/MPa	1.45
Coefficient of restitution grain-soil e	0.05
Coefficient of static friction grain-soil μ_s	1.25
Coefficient of rolling friction grain-soil μ_r	1.25
Coefficient of restitution grain-grain e	0.35
Coefficient of static friction grain-grain μ_s	0.3
Coefficient of rolling friction grain-grain μ_r	0.25
Coefficient of restitution grain-straw e	0.2
Coefficient of static friction grain-straw μ_s	0.8
Coefficient of rolling friction grain-straw μ_r	0.01
Coefficient of restitution grain-steel e	0.6
Coefficient of static friction grain-steel μ_s	0.5
Coefficient of rolling friction grain-steel μ_r	0.01

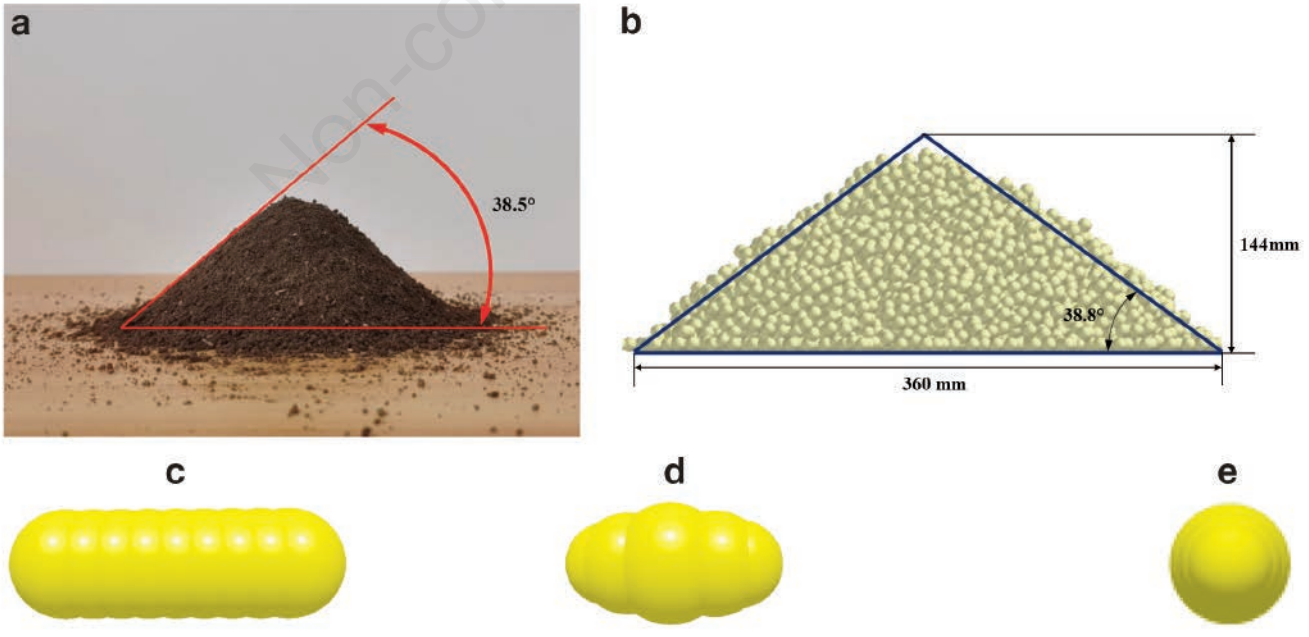

Figure 3. Calibration process. **a**) Soil accumulation angle actual; **b**) soil accumulation angle discrete element simulation; **c**) discrete element model of straw particles; **d**) wheat grain front view; **e**) side view.

Soil bin test

The experiment was conducted in the indoor soil bin of the Conservation Tillage Technology and Intelligent Equipment Innovation Laboratory at the Shandong University of Technology. The soil bin was 6 meters in length, 2 meters in width, and 0.7 meters in depth, and consisted of fluvo-aquic soil with an added appropriate amount of corn straw to simulate a straw-soil mixed environment. The soil moisture content was measured at 15.8% using the drying method, ensuring consistent test conditions throughout the plot.

Based on actual field environments, a two-layer soil model was established consisting of a bottom layer of pure soil particles with a depth of 150mm and a tillage layer mixed with soil and straw particles, having a depth of 50mm and a straw content of 30%. The depth of entry of the opener is 50 mm (Figure 4b). The operating conditions of the soil bin experiment were set to be the same as the simulation experiment, with the forward velocity of the opener being 5 km/h, the endpoint tangent angle being 108°, and the soil entry angle being 5°. The simulation results were compared with the actual data of the soil bin for the soil cover thickness and the straw ratio of the seed furrow.

The furrow side pick-up blade utilized in the experiment was fabricated using 3D printing technology and made of PLA material, with a manufacturing accuracy of 0.1mm. The remaining test equipment included a chisel opener, TYD-2 soil compaction meter, vernier caliper, tape measure, electronic scale, soil sampling ring knife, and drying oven.

Five locations were randomly selected observation areas in the operational travel stability zone of the test area (Figure 4c) and the soil height above the wheat seeds was measured using digital vernier calipers (resolution 0.02 mm) and the average value was obtained as the soil cover thickness. The results of the simulated test soil cover thickness were measured by measuring the height difference between the coordinates of wheat seeds and surface soil

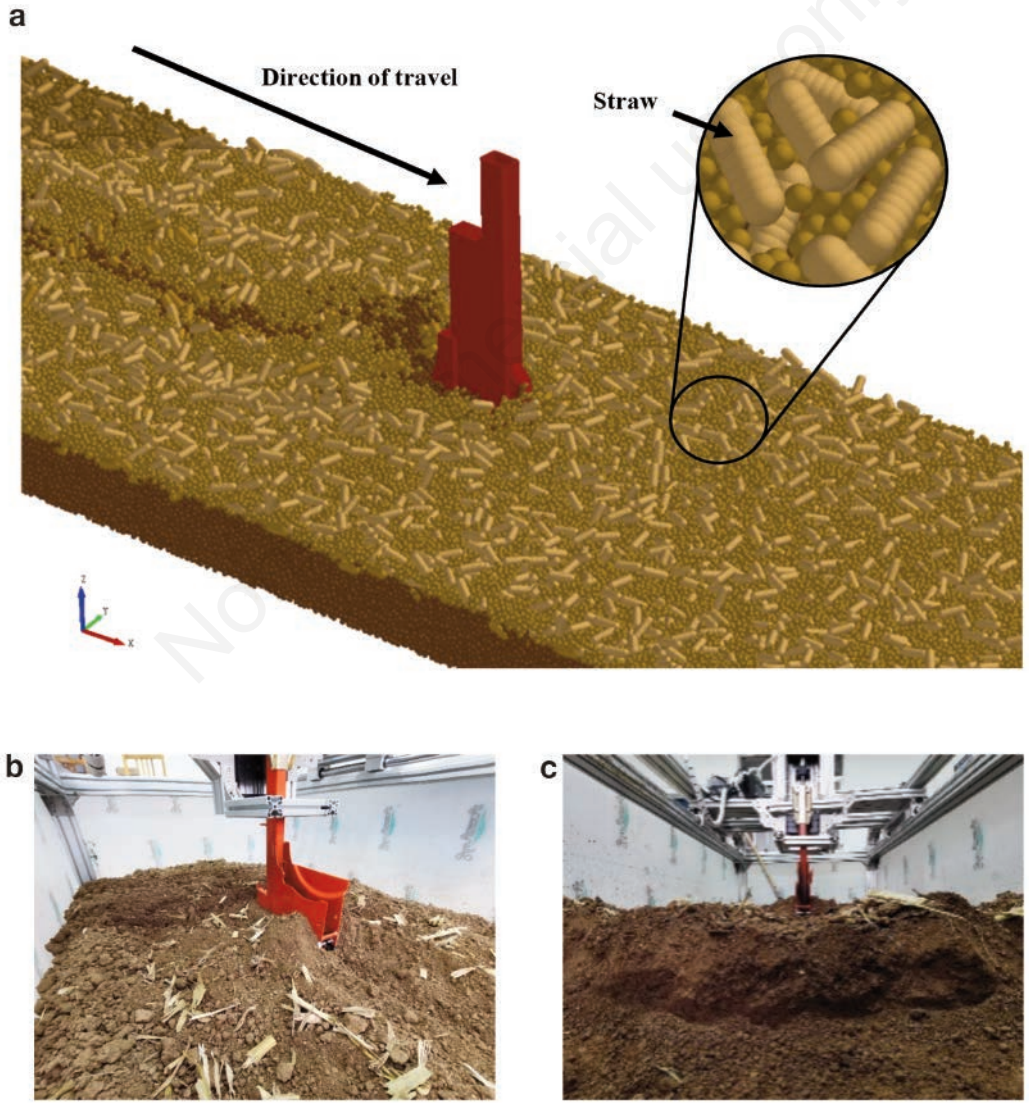

Figure 4. Experimentation. **a**) Axonometric view of opener through soil bin; **b**) test process; **c**) soil cover thickness measurement cross-section.

particles in the corresponding area selected by the EDEM post-processing module. The proportion of straw in the seed furrow, *i.e.*, the proportion of straw mass in the sampling area to all soil mass in the area, is the proportion of straw in the seed furrow, and the expression for the proportion of straw in the seed furrow is:

$$p = \frac{W_1}{W} \times 100\% \quad (7)$$

In the formula, ρ is the proportion of straw in the seed furrow, %

W_1 = Straw quality, g
W = the total mass of soil in the sampling area, g

After ditching in the test area, five sampling areas with the size of 300mm×200mm were randomly selected. The quality of soil and straw in the area was measured using a JA2003 electronic precision balance, and the five measurements were averaged. The straw mass and the total mass of the soil-straw complex in the selected area were derived from the EDEM post-processing module for calculation.

Experiment on optimal parameters of the furrow side pick-up blade

To further investigate the performance of the furrow side pick-up blade, the EDEM simulation model (Figure 4a) was used to determine the machine the forward velocity (v), the endpoint tangent angle (ω), and the soil entry angle (ε) as the test factors. The thickness of the covering soil and the ratio of straw in the seed furrow were used as evaluation indicators of the test. The optimal parameter combination for the furrow side pick-up blade was determined through a cross-rotation regression combination optimization test method. The codes for the test factors are presented in Table 4.

Results and Discussion

Model validation

DEM simulations were carried out using the software EDEM, 2020.0 (Academic Edition, Version: 6.0.0) working on a computer with AMD Ryzen 5 5600 G @ 3.90 GHz and 16.0 GB RAM.

The simulation results were compared with the results of the soil bin experiments. The average value of soil cover thickness predicted by the simulation experiment was 40.9 mm, and the average value of soil cover thickness measured by the soil bin test was 40.4 mm, with a single maximum error value of 2.26% (Figure 5a). The simulation test predicted a mean value of 17.69% of straw in the seed furrow, and the indoor soil bin test measured a mean value of 18.03% of straw in the seed furrow, with a single maximum error value of 2.86% (Figure 5b). The error of both results was within 5% and the trend was consistent, so it can be concluded that the model can better simulate the operation of the furrow opener.

Simulation process analysis

As illustrated in Figure 6a-b, the soil borrowing position of the furrow side pick-up blade is visually represented by setting the soil

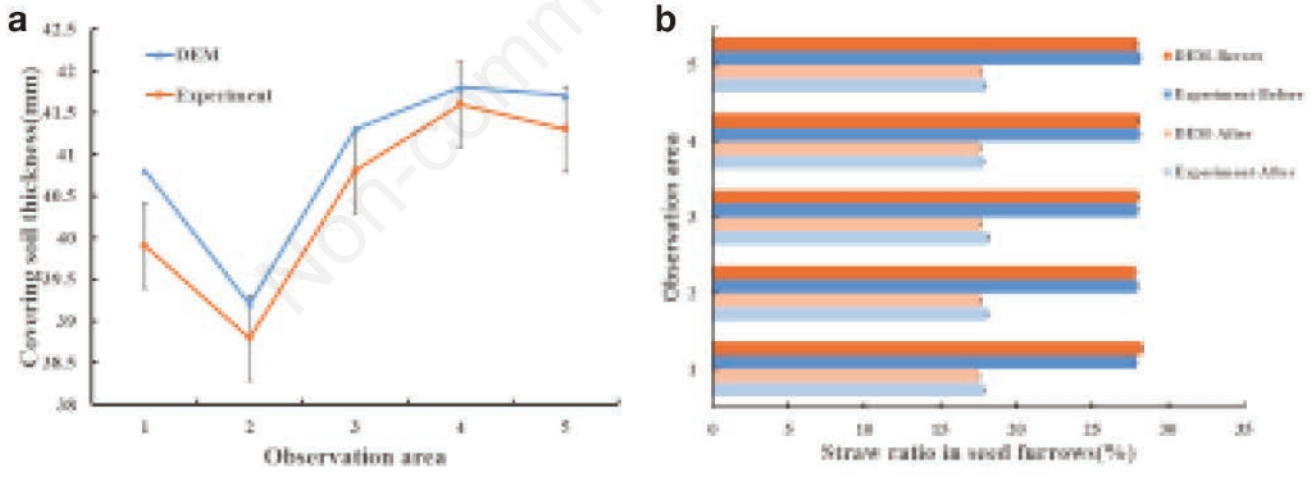

Figure 5. Comparison of discrete element simulation and indoor soil bin test for soil cover thickness and seed furrow straw ratio. **a)** Comparison of discrete element simulation of soil cover thickness and indoor soil bin test; **b)** comparison of discrete element simulation and indoor soil trough test for seed furrow straw ratio.

Table 4. Coding of experimental factors.

Factor level	Factor		
	Forward velocity v(km/h)	Endpoint tangent angle ω(°)	Angle of soil entry ε(°)
1	3	106	0
2	5	108	5
3	7	110	10

inside the seed furrow to orange, and the soil on the exterior of the seed furrow to khaki. By observing the change in color before and after the furrow side pick-up blade passes over the seed furrow, it can be determined that the blade extracts soil from both sides of the furrow, first covering the wheat seeds with khaki soil and then with orange soil from the seed furrow. This verifies the soil extraction position of the furrow side pick-up blade to be on the exterior of the seed furrow.

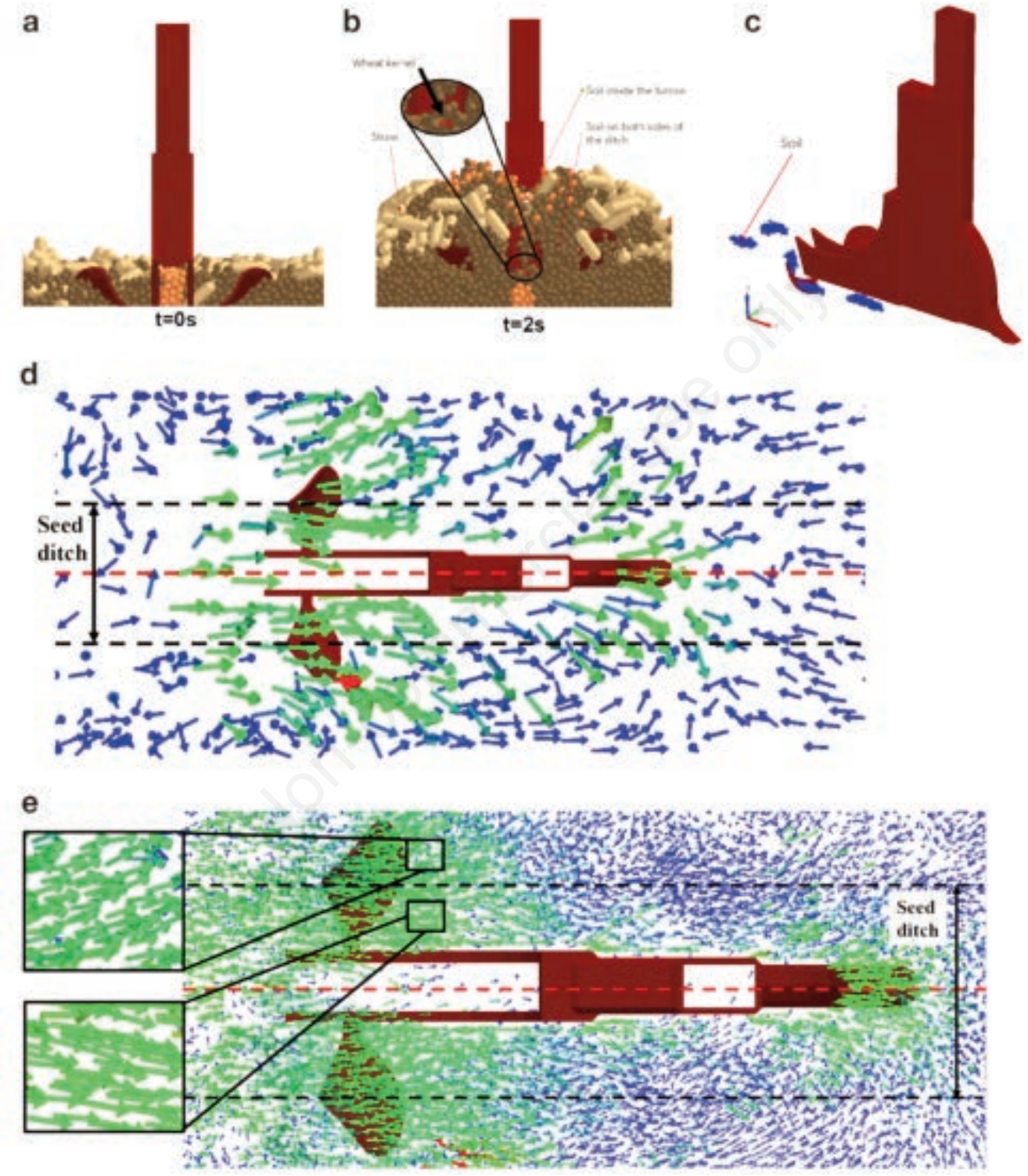

Figure 6. Analysis of simulation experiment process. **a**) Rear view of the opener through the soil at 0s; **b**) rear view of the opener through the soil at 2s; **c**) axonometric view of soil particle movement trend; **d**) vector diagram of the instantaneous velocity of straw particles (top view); **e**) vector diagram of the instantaneous velocity of soil particles (top view).

To investigate the movement pattern of soil particles as they pass through the furrow side pick-up blade, the particles on the side of the furrow adjacent to the opener were designated as blue for the purpose of observation. The movement trajectory of these selected soil particles is depicted in Figure 6c. As the furrow side pick-up blade passes through the blue soil particles on the furrow side, the particles are first lifted and then move in an upward, oblique direction along the curved surface. After reaching the highest point of the surface and being expelled, the soil particles begin to move towards the back of the opener due to inertia and then, under the influence of their gravity, exhibit a downward movement trend before finally falling into the seed furrow at the back of the opener. This motion law of the selected soil particles confirms the guiding effect of the surface of the furrow side pick-up blade on the soil on the furrow side, thereby demonstrating the design's feasibility.

In the EDEM simulation, the displacement and flow of particles as the opener moves through the furrow are represented by an instantaneous velocity vector diagram, where the magnitude of the particle velocity is indicated by its color. Figure 6d shows the vector diagram of the instantaneous velocity of the straw particles. It can be seen that the straw has two movement patterns after passing through the furrow side pick-up blade: it moves towards both sides of the seed furrow and falls into the seed furrow, or it continues to move forward with the furrow opener. From the comparison, it can be concluded that the proportion of straws moving to both sides of the seed furrow is relatively high at approximately 61.6%. The number of straws in the furrow is significantly reduced. Figure 6e shows the vector diagram of the instantaneous velocity of the soil particles. As can be seen from the enlarged image, the movement trends of the soil particles are similar to those of the straw particles, with roughly two movement patterns. Most of the soil particles move forward or into the furrow, which is approximately 68.4%. From this analysis it can be concluded that after the furrow-side pick-up blade operation, a larger number of straw particles accumulate on both sides of the seed furrow, while a significant proportion of the soil particles in the tillage layer on the furrow side accumulate inside the seed furrow, thus increasing the contact area between seed and soil in the furrow.

Trial protocol and results

The experimental program was executed through the EDEM software, and a total of 17 groups were conducted. The results of the measurements are presented in Table 5. A Box-Behnken test was applied to analyze the significance of the influence of the forward velocity (v) of the machine tool, the endpoint tangent angle (ω), and the angle of soil entry (ε) on the thickness of the cover soil and the proportion of straw in the seed furrow. The response model of the measurement index was obtained through regression equation fitting (Liu *et al.*, 2019). The simulation results were analyzed to identify the factors affecting the test indicators, and optimization of each combination was performed. Finally, a combination of test factors that were deemed more suitable was obtained.

Simulation results and analysis

The results in Table 5 were subjected to the significance and variance analysis using the Design-Expert software. A quadratic polynomial regression equation was selected and the stepwise regression method was employed to obtain the regression equation and perform the significance test.

Ansys of covering soil thickness

The concept of seed cover soil thickness refers to the thickness of the soil layer that covers the seeds, as depicted in Figure 7a. The test data were analyzed and fitted, and the results of the variance analysis of the cover soil thickness (H) are presented in Table 6.

It can be seen from Table 6 that X_2, X_3, X_2X_3, X_2^2, X_3^2 had highly significant effects on the covering soil thickness (H) ($p<0.01$); X_1, X_1^2, X_1X_2, X_1X_3 had significant effects on the covering soil thickness (H) ($0.01<p<0.05$). No factor was found to have a significant impact on the test index, which encompasses soil thickness (H) ($p>0.1$). The established regression model has a

Table 5. Test scheme and results.

No.	Forward velocity X_1 (Km/h)	Endpoint tangent angle X_2 (°)	Angle of soil entry X_3 (°)	Soil cover thickness H (mm)	Straw ratio in seed furrow (%)
1	7	108	10	41.331	23.509
2	7	110	5	41.919	23.574
3	5	108	5	41.556	21.941
4	5	106	10	31.247	22.448
5	5	106	0	33.769	22.597
6	5	108	5	43.890	21.833
7	5	110	10	40.889	22.506
8	3	110	5	33.487	22.549
9	5	108	5	42.060	21.258
10	7	106	5	33.770	22.536
11	3	108	0	35.990	23.583
12	5	108	5	40.155	21.246
13	5	110	0	32.271	23.325
14	5	108	5	42.869	21.386
15	3	106	5	33.639	22.571
16	7	108	0	33.641	23.845
17	3	108	10	36.528	22.971

P-value of less than 0.001, which demonstrates that the relationship between the dependent variable and all the independent variables in the model is highly significant. The P-value of 0.5203 for the lack of fit item is greater than 0.1, indicating that the lack of fit is not statistically significant. This result suggests that the regression model is an appropriate fit for the simulation test results. Therefore, the regression equation of the influence of each factor on the covering soil thickness H is obtained:

$$Y_1 = 42.11 + 1.38x_1 + 2.02x_2 + 1.79x_3 + 2.08x_1x_2 + 1.79x_1x_3 + 2.78x_2x_3 - 2.04x_1^2 - 4.37x_2^2 - 3.2x_3^2 \quad (8)$$

Analysis of the proportion of straw in seed furrows

The straw content in the seed furrow is indicative of the distribution of straw in the soil that covers the furrow, as depicted in Figure 7b. A statistical analysis was performed on the test data to determine the variability of the straw content in the seed furrow. The results of this analysis are presented in Table 7 through the use of variance analysis.

The results presented in Table 7 demonstrate that variables X_1^2 and X_3^2 have a highly significant effect ($p<0.01$) on the straw content in seed furrows. Meanwhile, variables X_1, X_2, and X_3 exhibit a significant effect ($0.01<p<0.05$) on the straw content. The remaining factors have no statistically significant impact ($p>0.1$) on the straw content in seed furrows as per the test index. The established regression model has a highly significant relationship ($p<0.001$) between the dependent variable and all independent variables. Additionally, the lack of fit, as indicated by the P-value of 0.9709 ($p>0.1$), is not statistically significant, implying that the regression model is a good fit for the simulation test results. Therefore, the regression equation of the influence of various fac-

Table 6. Variance analysis of covering soil thickness.

Parameter	Sum of squares	Degrees of freedom	Sum of mean squares	F	P
Model	289.8	9	32.2	17.19	0.0006**
X_1	15.17	1	15.17	8.1	0.0248*
X_2	32.57	1	32.57	17.39	0.0042**
X_3	25.65	1	25.65	13.69	0.0077**
X_1X_2	17.23	1	17.23	9.2	0.019*
X_1X_3	12.79	1	12.79	6.83	0.0348*
X_2X_3	31.02	1	31.02	16.56	0.0047**
X_1^2	17.47	1	17.47	9.33	0.0185*
X_2^2	80.24	1	80.24	42.84	0.0003**
X_3^2	43.03	1	43.03	22.97	0.002**
Residual	13.11	7	1.87		
Lack of fit	5.24	3	1.75	0.8864	0.5203
Pure error	7.88	4	1.97		
Cor total	302.91	16			

*significant ($p<0.05$); **very significant ($p<0.01$).

Table 7. VAnalysis of variance for the proportion of straw in various furrows.

Parameter	Sum of squares	Degrees of freedom	Sum of mean squares	F	P
Model	10.66	9	1.18	18.01	0.0005**
X_1	0.4465	1	0.4465	6.79	0.0351*
X_2	0.4522	1	0.4522	6.88	0.0343*
X_3	0.4589	1	0.4589	6.98	0.0333*
X_1X_2	0.2304	1	0.2304	3.5	0.1034
X_1X_3	0.019	1	0.019	0.2896	0.6071
X_2X_3	0.1122	1	0.1122	1.71	0.2327
X_1^2	4.24	1	4.24	64.53	<0.0001**
X_2^2	0.2545	1	0.2545	3.87	0.0898
X_3^2	3.72	1	3.72	56.63	0.0001**
Residual	0.4602	7	0.0657		
Lack of fit	0.0242	3	0.0081	0.0739	0.9709
Pure error	0.4361	4	0.109		
Cor total	11.12	16			

*significant ($p<0.05$); **very significant ($p<0.01$).

tors on the proportion of straw in the seed furrow is obtained:

$$Y_2 = 21.53 + 0.2363x_1 + 0.2377x_2 - 0.2395x_3 + 0.24x_1x_2 + 0.069x_1x_3 - 0.1675x_2x_3 + x_1^2 + 0.2459x_2^2 + 0.9403x_3^2 \quad (9)$$

Response surface analysis

The response surface is a graphical representation of the relationship between two interacting experimental factors and the response value when all other factors are held constant. The degree of influence of the two experimental factors on the response value is evaluated based on its slope. Through data processing using the Design-Expert software, the response surface for the significant and relatively significant interactions between the forward velocity (X_1), the endpoint tangent angle (X_2), and the angle of soil entry (X_3) on the cover soil thickness (H) and the proportion of straw in the seed furrow was derived, as demonstrated in Figure 8a-b.

Figure 8a depicts the interaction between the forward velocity, the endpoint tangent angle, and the angle of soil entry on the overburden thickness. It is evident that each factor has a significant impact on the soil cover thickness.

As shown in Figure 8a, when the forward velocity is kept constant, the soil cover thickness initially increases and then decreases with an increase in the endpoint tangent angle. The optimal endpoint tangent angle range is 107.8° to 109.5°. Similarly, when the endpoint tangent angle is held constant, the soil cover thickness increases initially and then decreases with an increase in the forward velocity, with an optimal forward velocity range of 4.7 km/h to 6.8 km/h. When the forward velocity is at its lowest and the endpoint tangent angle is at its highest, the soil cover thickness is at its minimum. The slope of the forward velocity is steeper than that of the endpoint tangent angle, indicating that the effect of the forward velocity is more significant.

As depicted in Figure 8a2, the relationship between the forward velocity, the endpoint tangent angle, and the angle of soil entry on overburden thickness is further explored. When the forward velocity is kept constant, the soil cover thickness first increases and then decreases with the increase of the angle of soil entry, with the optimal range of the angle of soil entry being 4.8° to 9.0°. On the other hand, when the angle of soil entry is constant, the soil cover thickness increases initially and then decreases with an increase in forward velocity, and the optimal range of the for-

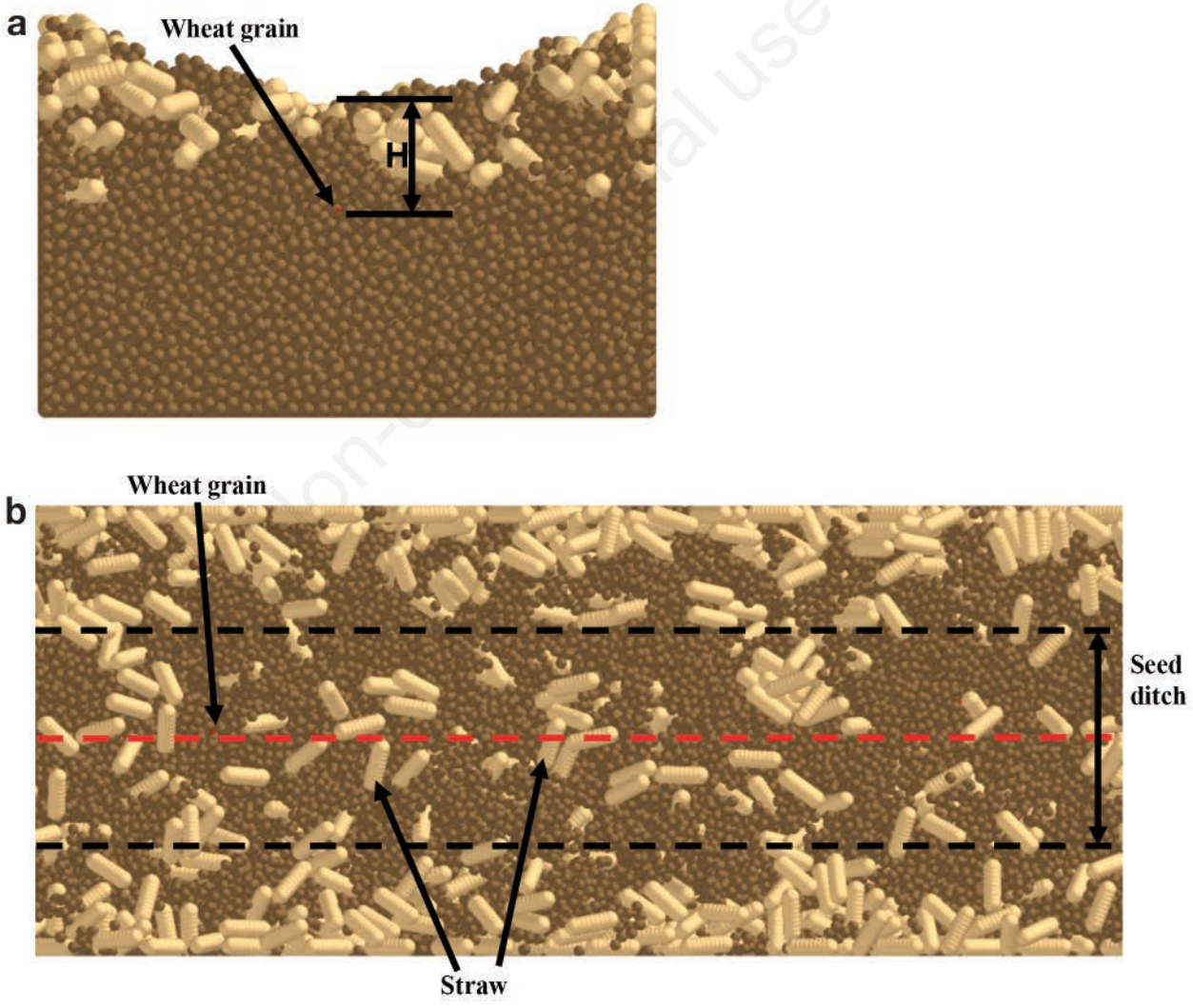

Figure 7. Simulation experiment results. **a**) Schematic diagram of covering soil thickness; **b**) distribution map of straw in various furrows.

ward velocity is found to be 5.1 km/h to 6.3 km/h. As the angle of soil entry decreases and the forward velocity increases, the soil cover thickness reaches its minimum. The slope of the forward velocity is steeper than that of the angle of soil entry, indicating a more significant effect of the forward velocity on the soil cover thickness. Furthermore, Figure 8a3 provides insight into the relationship between the endpoint tangent angle and the angle of soil entry on overburden thickness. When the endpoint tangent angle is held constant, the soil cover thickness first increases and then decreases with the increase of the angle of soil entry, with the optimal range of the angle of soil entry being 5.0° to 9.3°. When the angle of soil entry is kept constant, the soil cover thickness increases initially and then decreases with the increase in endpoint tangent angle, and the optimal range of the endpoint tangent angle is found to be 108.2° to 109.4°. The soil cover thickness reaches its minimum when the endpoint tangent angle is the smallest and the angle of soil entry is the largest. As depicted in Figure 8b, the interaction between various factors, including the forward velocity, endpoint tangent angle, and angle of soil entry, on the ratio of seed furrow straw is presented. With regards to Figure 8b1, when the forward velocity is held constant, the proportion of straw in the seed furrow first decreases and then increases with an increase in the endpoint tangent angle. The optimal endpoint tangent angle range, in this case, lies between 106.4° and 108.3°. When the endpoint tangent angle is held constant, the proportion of straw in the seed furrow decreases first and then increases with the increase in forward velocity, and the optimal forward velocity range is 4.4 km/h to 5.2 km/h. The proportion of straw in the seed furrow is found to be the smallest when both the forward velocity and the endpoint tangent angle take the middle value. The influence of the endpoint tangent angle is found to be more significant as the slope of the endpoint tangent angle is steeper as compared to the forward velocity.

Similarly, as shown in Figure 8b2, when the forward velocity is held constant, the proportion of straw in the seed furrow decreases first and then increases with the increase in the angle of soil entry. The optimal range of the angle of soil entry, in this case, is 4.4° to 7.2°. When the angle of soil entry is held constant, the proportion of straw in the seed furrow decreases first and then increases with an increase in forward velocity, and the optimal forward velocity range is 4.1 km/h to 5.2 km/h. The proportion of straw in the seed furrow is found to be the smallest when both the angle of soil entry and the forward velocity take the middle value, and the impact of forward velocity is found to be more significant as the slope of the forward velocity is steeper as compared to the angle of soil entry. Lastly, as depicted in Figure 8b3, when the endpoint tangent angle is held constant, the proportion of straw in the seed fur-

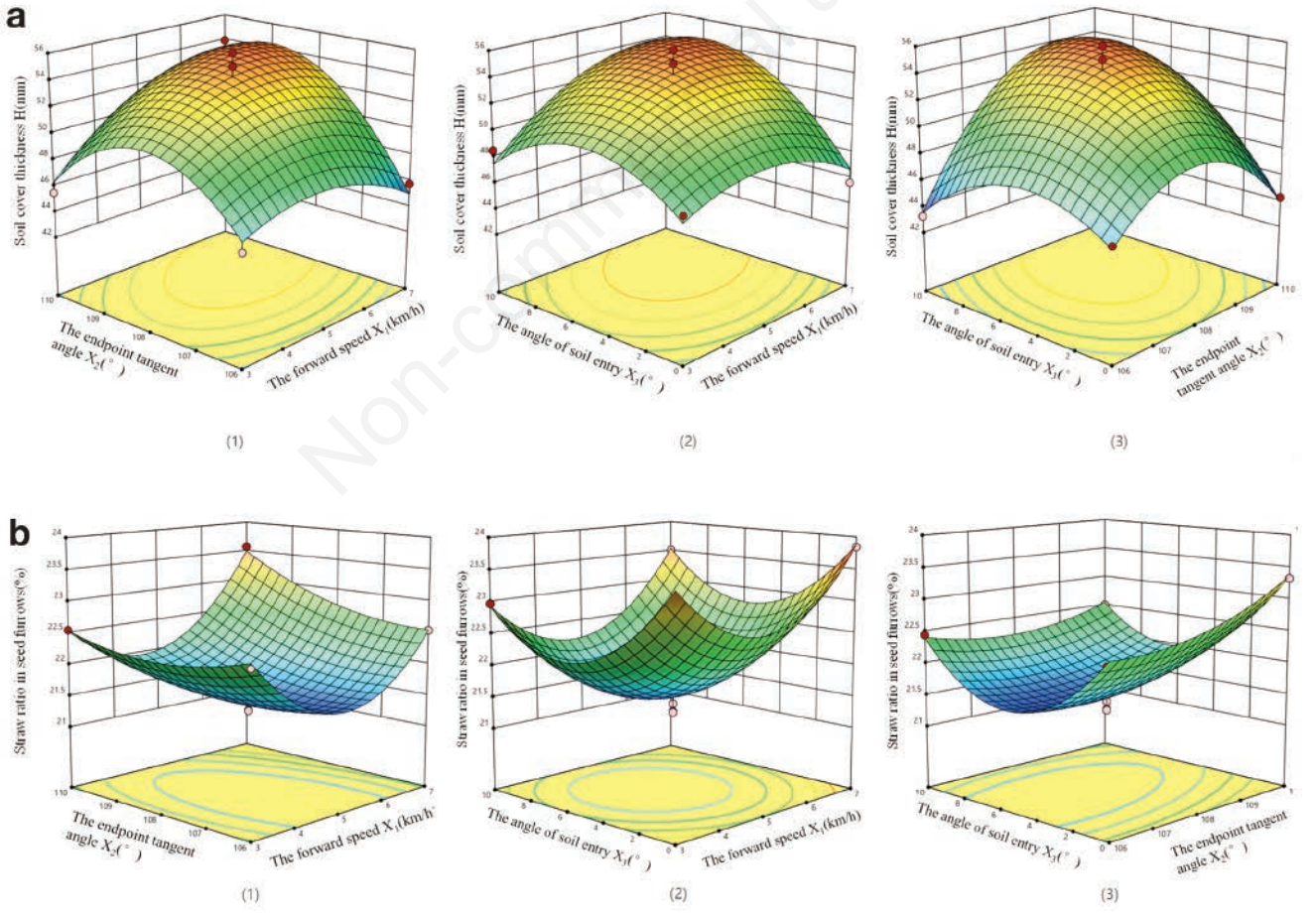

Figure 8. Response surface. **a**) The influence of test factors on the thickness of the covering soil; **b**) the experimental factors affecting the proportion of straw in seed furrows.

row decreases first and then increases with an increase in the angle of soil entry, and the optimal range of the angle of soil entry is 4.2° to 6.6°. When the angle of soil entry is held constant, the proportion of straw in the seed furrow decreases first and then increases with an increase in the endpoint tangent angle, and the optimal endpoint tangent angle range is 106.4° to 107.8°. The proportion of straw in the seed furrow is found to be the smallest when the endpoint tangent angle takes the smaller value and the angle of soil entry takes the middle value, and the influence of the endpoint tangent angle is found to be more significant as the slope of the endpoint tangent angle is steeper as compared to the angle of soil entry. In this study, the optimization of the combination of test factor levels was performed through the analysis of six response surfaces using Design-Expert software. Based on agronomic requirements and simulation experiments, it was determined that the optimal soil stress value is achieved when the straw content in the soil is within the range of 10% to 30%. Thus, in this study, the lowest straw content was established as the optimization target, and the optimal constraint condition was set as a covering soil thickness of no greater than 40mm. Among the multiple sets of optimized parameter combinations obtained, a set of optimal parameters was selected, which included a forward velocity of 4.86 km/h, an endpoint tangent angle of 107.17°, and an angle of soil entry of 5.46°. These parameters were determined to result in the ideal performance of the furrow side pick-up blade. It was predicted that the covering soil thickness would be 40 mm, with a proportion of straw in the seed furrow of 21.46%.

Conclusions

First, the interaction model of soil-straw- the furrow side pick-up blade established through the DEM offers a viable technical solution for addressing the seed-soil contact problem under straw cover. Among the factors affecting the proportion of straw in the furrow, forward velocity, Endpoint tangent angle, and angle of soil entry exhibit significant effects, with the square terms of forward velocity and angle of soil entry demonstrating highly significant impacts. Other factors do not significantly affect the experimental indicator, the proportion of straw in the furrow.

Through response surface analysis, we have determined the extent of the influence of forward velocity, Endpoint tangent angle, and angle of soil entry on burial depth and the proportion of straw in the furrow.

Finally, the optimal operational parameter combination consists of a forward velocity of 4.86 km/h, an Endpoint tangent angle of 107.17°, and angle of soil entry of 5.46°. Under these conditions, the soil exhibits the lowest straw content, a burial depth of 40 mm, and a proportion of straw in the furrow of 21.46%.

These findings provide crucial guidance for understanding the interactions between agricultural machinery components, straw, and soil, offering valuable insights for practical field operations. In future research and real-world applications, these conclusions can inform the selection of optimal operating parameters to enhance the performance and efficiency of agricultural machinery. This study provides robust support for addressing critical issues in field operations and holds significant relevance for the sustainable development of modern agriculture.

References

Aikins K.A., Barr J., Ucgul M., Jensen T., Antille D.L., Desbiolles J.M.A. 2020. No-tillage furrow opener performance: A review of tool geometry, settings and interactions with soil and crop residue. Soil Res. 58:603-21.

Bai L., Huang Y., Gao P., Ding S., Zhang H., Fu Z., Zhu R. 2020. Design and test of seed and fertilizer separate device based on double disc covering soil. J. Northwest A & F University (Natural Science Edition). 1:135-45+154.

Barker M.E., Plouffe C. 2017. Simulation of Planter Row Cleaner in Corn Residue Using Discrete Element Modeling. ASABE Annual International Meeting (p. 1).

Chandio F.A. 2013. Interaction of straw-soil-disc tool under controlled conditions. Unpublished thesis (PhD), of Nanjing Agricultural University, China.

Chen H., Hou L., Hou S., Li Y., Min S., Chai Y. 2018. Design and Optimization Experiment of Anti-blocking Mechanism of No-tillage Planter for Grand Ridge with Raw Corn Stubble. Trans. Chin. Soc. Agric. Machin. 8:59-67.

Ding Q., Ren J., Belal E.A., Zhao J., Ge S., Li Y. 2017. DEM Analysis of Subsoiling Process in Wet Clayey Paddy Soil. Trans. Chin. Soc. Agric. Machin. 3:38-48.

Fu S.Y., Feng X.Q., Lauke B., Mai Y.W. 2008. Effects of particle size, particle/matrix interface adhesion and particle loading on mechanical properties of particulate–polymer composites. Compos. B. Eng. 39:933-61.

Gu F., Hu Z., Chen Y., Wu F. 2016. Development and experiment of peanut no-till planter under full wheat straw mulching based on "clean area planting". Trans. Chin. Soc. Agric. Eng. 20:15-23.

Itasca C.G.I. 2005. PFC3D (Particle Flow Code in Three Dimensions). Minneapolis, Minnesota, USA.

Liu F., Jian Z., Chen J. 2018a. Modeling of flexible wheat straw by discrete element method and its parameter calibration. Int. J. Agric. Biol. Eng. 11:42-6.

Liu J., Wang H., Wang Q., Li S., Li H., He J. 2018b. Design and experiment of strip cleaning device of no and minimum-tillage corn seeder. Transact. CSAM. 49:132-40.

Liu F., Zhang J., Li B., Chen J. 2016. Calibration of parameters of wheat required in Discrete Element Method simulation based on repose angle of particle heap. Trans. Chin. Soc. Agric. Eng. 12:247-53.

Liu X., Zhang Q., Liu L., Wei G., Xiao W., Liao Q. 2019. Surface Optimization of Ship Type Ditching System Based on Differential Geometry and EDEM Simulation. Trans. Chin. Soc. Agric. Machin. 8:59-69.

Lu H., Feng Y., Gao Q., Xing J., Chen Y., Yang L., Xue L. 2020. Surface soil mixing is more beneficial than the plough layer mixing mode of biochar application for nitrogen retention in a paddy system. Sci. Total Environ. 718:137399.

Lv J., Liu Q., Li Z., Li J., Liu Z. 2021. Design and Experiment of Soil Cultivating Device of Plowshare Potato Field Cultivator. Trans. Chin. Soc. Agric. Machin. 7:71-82.

Niu Q., Wang Q., Chen L., Li H., He J., Li W. 2017. Design and experiment on straw post-covering wheat planter. Trans. Chin. Soc. Agric. Machin. 48:52-9.

Shi L., Zhao W., Sun W. 2017. Parameter calibration of soil particles contact model of farmland soil in northwest arid region based on discrete element method. Trans. Chin. Soc. Agric. Eng. 33:181-7.

Sun K., Yu J., Liang L., Wang Y., Yan D., Zhou L., Yu Y. 2022. A DEM-based general modelling method and experimental veri-

fication for wheat seeds. Powder Technol. 401:117353.
Sun L., Gibson R.F., Gordaninejad F., Suhr J. 2009. Energy absorption capability of nanocomposites: a review. Compos. Sci. Technol. 69:2392-409.
Wang X., Hu H., Wang Q., Li H., He J., Chen W. 2017. Calibration Method of Soil Contact Characteristic Parameters Based on DEM Theory. Trans. Chin. Soc. Agric. Machin. 12:78-85.
Wei G., Zhang Q., Liu L., Xiao W., Sun W., Liao Q. 2020. Design and Experiment of Plowing and Rotary Tillage Buckle Device for Rapeseed Direct Seeder. Trans. Chin. Soc. Agric. Machin. 6:38-46.
Wu T., Huang W., Chen X., Ma X., Han Z., Pan T. 2017. Calibration of discrete element model parameters for cohesive soil considering the cohesion between particles. J. South Chin. Agric. Univ. 38:93-8.
Xiong P., Yang Z., Sun Z., Zhang Q., Huang Y., Zhang Z. 2018. Simulation analysis and experiment for three-axis working resistances of rotary blade based on discrete element method. Trans. Chin. Soc. Agric. Eng. 18:113-21.
Yu J., Lu C., Wei R., Fu X., Li K., Tang Z., Wang F. 2018. Simulation test of performance of wheat precision seed-metering device based on Discrete Element Method. Jiangsu Agric. Sci. 8:225-8.
Zhai L. 2011. Study on the effects of plough's working and structure parameters on its resistance under rheological soil conditions. PH.D. Nanjing Agric. Univ. Chin.
Zhang K., Huang J., Yang M., Zhang F., Huang X., Zhao C. 2010. Finite element analysis and experimental verification of wheat grain under compression loads. Trans. Chin. Soc. Agric. Eng. 6:352-6+391.
Zhang R., Li J., Li Y., Liu Z., Chen B. 2009. DEM macroscopic and mesoscopic analysis in disturbed behavior of soil acted by part with complex surface. J. Jilin Univ. Eng. Technol. Ed. 5:1218-23.
Zhang T., Liu F., Zhao M., Ma Q., Wang W., Fan Q., Yan P. 2018. Determination of corn stalk contact parameters and calibration of Discrete Element Method simulation. J. Chin. Agric. Univ. 4:120-7.
Zhang Z., He J., Li H., Wang Q., Ju J., Yan X. 2017. Design and Experiment on Straw Chopper Cum Spreader with Adjustable Spreading Device. Trans. Chin. Soc. Agric. Machin. 9:76-87.
Zhao H., He J., Li H., Liu C., Zheng K., Zhang Z. 2018a. Design and Experiment of Strip Rotary-cut-throw Anti-blocking Implement. Trans. Chin. Soc. Agric. Machin. 5:65-75.
Zhao H., He J., Li H., Mao Y., Liu P. 2018b. Comparison on soil, straw disturbance, and resistance of conventional and plain-straight blade for strip-tillage with Discrete Element Method. Int. Agric. Eng. J. 27:229-40.
Zhao L., Zhang Z., Wang C., Jian S., Liu T., Cui D., Ding X. 2018c. Design of monitoring system for wheat precision seeding-fertilizing machine based on variable distance photoelectric sensor. Trans. Chin. Soc. Agric. Eng. 13:27-34.
Zhao H., He J., Zheng Z., Zhang Z., Liu W. 2020. Strip Tillage Inter-row Residue Side-throwing Device of No/minimum-till Seeder for Anti-blocking and Seedbed-cleaning. Trans. Chin. Soc. Agric. Machin. 12:24-34.
Zhao S., Liu H., Yang C., Yang L., Gao L., Yang Y. 2021. Design and Discrete Element Simulation of Interactive Layered Subsoiler with Maize Straw Returned to Filed. Trans. Chin. Soc. Agric. Machin. 3:75-87.
Zhao S., Wang J., Yang C., Chen J., Yang, Y. 2019. Design and Experiment of Stubble Chopper under Conservation Tillage. Trans. Chin. Soc. Agric. Machin. 9:57-68.
Zhong X., Zhang X., Geng Y., Wei Z., Cheng X., Wang X. 2023. Research on Load Transfer of Straw-soil Complex Based on Discrete Element Method. J. Agric. Mechan. Res. 3:17-24.